Mississippi State University

Scholars Junction

12-13-2003

Probabilistic Design Optimization of Built-Up Aircraft Structures with Application

Qiulin Xie

Follow this and additional works at: https://scholarsjunction.msstate.edu/td

Recommended Citation

PROBABILISTIC DESIGN OPTIMIZATION OF BUILT-UP AIRCRAFT

STRUCTURES WITH APPLICATION

By

Qiulin Xie

A Thesis
Submitted to the Faculty of
Mississippi State University
in Partial Fulfillment of the Requirements
for the Degree of Master of Science
in Aerospace Engineering
in the Department of Aerospace Engineering

Mississippi State, Mississippi

December 2003

PROBABILISTIC DESIGN OPTIMIZATION OF BUILT-UP AIRCRAFT

STRUCTURES WITH APPLICATION

By

Qiulin Xie

Approved:

_____   _____
Masoud Rais-Rohani   James C. Newman, Jr.
Professor of Aerospace   Professor of Aerospace
 Engineering   Engineering
(Director of Thesis)   (Committee Member)

_____   _____
Christopher D. Eamon   Pasquale Cinnella
Assistant Professor of Civil   Professor of Aerospace
Engineering   Engineering
(Committee Member)   (Graduate Coordinator)

_____
A. Wayne Bennett
Dean of the College of Engineering

Name: Qiulin Xie

Date of Degree: December 13, 2003

Institution: Mississippi State University

Major Field: Aerospace Engineering

Major Professor: Dr. Masoud Rais-Rohani

Title of Study: PROBABILISTIC DESIGN OPTIMIZATION OF AIRCRAFT
STRUCTURES WITH APPLICATION

Pages in Study: 94

Candidate for Degree of Master of Science

This thesis discusses a methodology for probabilistic design optimization of aircraft structures subject to a multidisciplinary set of requirements originating from the desire to minimize structural weight while fulfilling the demands for quality, safety, producibility, and affordability. With this design methodology as the framework, a software is developed, which is capable of performing design optimization of metallic built-up beam structures where the material properties, external load, as well as the structural dimensions are treated as probabilistic random variables. The structural and failure analyses are based on analytical and semi-empirical methods whereas the component reliability analysis is based on advanced first-order second moment method. Metrics-based analytical models are used for the manufacturability analysis of individual parts with the total manufacturing cost estimated using models derived from the manufacturing cost / design guide developed by the Battelle's Columbus Laboratories. The resulting optimization problem is solved using the method of sequential quadratic

programming. A wing spar design optimization problem is used as a demonstrative example including a comparison between non-buckling and buckling web design concepts. A sensitivity analysis is performed and the optimization results are used to highlight the tradeoffs among weight, reliability, and manufacturing cost.

ACKNOWLEDGEMENTS

TABLE OF CONTENTS

Page

LIST OF TABLES

LIST OF FIGURES

CHAPTER I

INTRODUCTION

1.1 Review of Literature on Producibility Analysis

One major drawback in traditional design environment is often the scarcity of communication between design and manufacturing engineers at the early product design phase. In that environment, the design engineer is mainly concerned with product functionality and producibility, defined as the ease with which a product can be manufactured, may not receive much attention. Consequently, manufacturing related problems may not be discovered until later when a design change will often result in prohibitive measures and delayed lead-time [1], both of which are detrimental to the survival of an enterprise under current harsh competition pressures.

The need to address the manufacturing requirements in early stages of product design has prompted the development and application of design for manufacture (DFM) and assembly (DFMA) methodologies that focus on component manufacturing processes and methods of assembly [2].

The activities in this area can be broadly categorized as 1) Strategies and procedures for integrated product and process design and development, 2) Manufacturability analysis with focus on a specific process, and 3) Design

optimization with manufacturing constraints. Some examples in each category are provided below.

Kessler et al. [3] describe producibility methodology and virtual manufacturing as effective means of addressing manufacturing requirements in product design. Their strategy is based on a hierarchical producibility framework focusing on critical components and manufacturing processes. Virtual manufacturing is used for computer modeling of key manufacturing processes and functions that are defined as constraints from the standpoint of capacity or capability. El-Gizawy et al. [4] proposed a strategy for integrating product and process design based on a knowledge-based expert system that contains information related to the capabilities of various manufacturing processes. By examining the product-specific constraints associated with mechanical properties, geometric shape, and dimensional accuracy and the knowledge about process capabilities, an iterative procedure is used resulting in a desired match between product design and the most efficient manufacturing process.

Manufacturability analysis is an active area of research. In order to facilitate the implementation of DFM, a series of studies associated with many manufacturing processes have been conducted. In terms of cost, Boothroyd et al [5] proposed cost estimation models for machined components during the conceptual design phase. The feedback is quantitative metrics, but the rough classification on which that cost estimation is based is not appropriate for components whose geometry significantly deviate from that listed in the paper. Based on group technology and manufacturing features identification techniques, Hu and Polia [6] developed an approach to determine manufacturability by estimation of manufacturing cost. Comparisons were made among

injection molding, stamping, and assembling to determine which process has the highest manufacturability using the proposed approach. For machined parts, Gupta [7] developed a manufacturability analysis system. In this approach, machining plans are generated by machining features recognition. The production time is estimated if a plan can produce the desired design tolerance. The manufacturability of the part is obtained as the minimum production time for all generated plans that meet tolerance specifications. The part cannot be machined if no generated plans can meet tolerance constraints.

Gupta et al. [1] describe some of the manufacturability analysis techniques and the efforts that are underway to automate them. Subramaniam and Ulrich [8] presented an approach for quantitative analysis of producibility based on the physics of the extrusion process and parameters on which it depends. They identify the failure modes encountered in the extrusion process and describe the metrics that could be used to alleviate them. Shankar and Jansson [9] developed a generalized methodology for the manufacturability analysis of a generic product based on five core manufacturability concepts and the hierarchy of factors on which they depend. Some of the recommended factors in that research were subsequently used by Rais-Rohani [10] to develop quantitative manufacturability indices for built-up aircraft structures. The Six-Sigma producibility analysis suggested by Harry and Lawson[11] offers a statistical approach, which could be used to link manufacturing process variability to overall product producibility and robustness.

Many general design rules and principles have been suggested to reduce or eliminate problems encountered during product manufacture. However, because of

their qualitative nature and broadness, it is difficult or impracticable to integrate many of these design rules into a design optimization framework. To alleviate this weakness, many researchers have developed what could be characterized as physics based modeling of the manufacturing process

In this thesis, metrics-based producibility models [8] are used to introduce process-specific manufacturability constraints to relate process requirements to structural design variables controlled in the design process. Details of this methodology are discussed later in the application of this methodology to an example problem.

1.2 Review of Literature on Reliability Analysis

Most approaches dealing with structural reliability can be generalized into analytical and simulation techniques. These techniques have been applied to obtain a reliability index or probability of failure for a structural component with only one failure mode or a structural system or component with several failure modes.

Simulation techniques mainly include direct Monte Carlo simulation (MCS) as well as many variance-reduction methods including Stratified Sampling, Importance Sampling, and Adaptive Importance Sampling (AIS), etc. The MCS technique was originally suggested in the early 1940's to test engineering systems using inexpensive simulation technique [12]. The application of MCS to compute the probability of failure of a structure was demonstrated by Shinozuka [13].

In Monte Carlo scheme [12], the probability of failure, P_f can be estimated by

$$P_f = \frac{N_f}{N} \qquad (1.1)$$

where N_f is the number of simulations resulting in failure and N is the total number

of simulation cycles. The statistical accuracy of the estimated probability of failure is

measured by its coefficient of variation $Cov(P_f)$ as

$$Cov(P_f) = \frac{\sqrt{\dfrac{(1-P_f)P_f}{N}}}{P_f} \tag{1.2}$$

Equation (1.2) indicates that a small probability of failure will necessitate a huge

number of simulation cycles to keep the accuracy at an acceptable level. This usually

results in an increase in computational cost. Also for a practical problem with many

random variables, MCS becomes prohibitively expensive. To overcome the

deficiency of MCS, several more efficient alternative methods such as Importance

Sampling (IS) method [12] have been developed. The basic strategy for IS is to

generate random variables using different probability distributions whose mean

values are closer to the design point than that of the original probability distribution.

Therefore, simulation efficiency is increased since failures are obtained more

frequently than before.

Harbitz and Veritas [14] presented a general procedure based on IS technique to

compute the probability of failure, and applied this procedure to a fatigue problem. It

was shown that IS was much more efficient than MCS simulation while keeping the

same accuracy.

The commonly used analytical techniques for structural reliability analysis

include the first and second-order reliability methods [FORM and SORM]. The basic

idea behind these techniques is to transform the original random variables into a set of

uncorrelated random variables in standardized normal space, and then either FORM

or SORM is used to approximate the limit state function describing the failure criterion. The probability of failure of the component is estimated in terms of $\boldsymbol{b}$ such that $P_f \approx \Phi(-\boldsymbol{b})$, where Φ is the cumulative distribution function of a standard normal variable.

To evaluate reliability index in FORM, Hasofer and Lind [15] suggested an iterative algorithm in which the limit state surface is approximated by a tangent hyper plane at the design point that will eventually converge to the most probable point (MPP) of failure. The reliability index defines the shortest distance from the origin of the transformed coordinate system to the limit state surface. Rackwitz and Fiessler [16] extended this algorithm by incorporating distribution information. The algorithms of Hasofer and Lind along with that of Rackwitz and Fissler are jointly called HL-RF algorithm.

A FORM-based approach to compute system reliability was due to Hohenbichler and Rackwitz [17]. They first reduced the system to a series of parallel systems, then gave a first-order solution to the multi-normal integral for simple series or parallel systems, and finally determined the failure probability of the minimal cut set (parallel subsystems in series) using bounds for the union of events. Gollwitzer and Rackwitz [18] simplified the estimation of system reliability by replacing subsystems with equivalent components under the framework of FORM.

Enevoldsen and Sorensen [19] described a FORM-based procedure to calculate the system reliability index by modeling the system as a series system of parallel systems. The correlations between and within parallel systems have been taken into

account to obtain the system reliability index as well as the reliability sensitivity analysis.

FORM is usually accurate for limit state functions that are not highly nonlinear. SORM has been proposed to improve the reliability estimation by using a quadratic approximation of the limit state surface for highly nonlinear limit state functions. Such an approximation was initially investigated by Fiessler et al. [20]. Breitung [21] has suggested an important asymptotical procedure to predict failure probabilities for large $\boldsymbol{b}$ by applying quadratic approximation at MPP. It has been shown that the probability of failure can be expressed as

$$P_f \approx \Phi(-\boldsymbol{b})\prod_{i=1}^{n-1}(1-\boldsymbol{b}\frac{\boldsymbol{f}(-\boldsymbol{b})}{\Phi(-\boldsymbol{b})}\boldsymbol{k}_i)^{1/2}, \boldsymbol{b} \to \infty \tag{1.4}$$

Where $\boldsymbol{k}_i$ are the main curvatures of the failure surface at MPP.

Tvedt [22] offered an exact probability of failure for both parabolic and the general second order approximation at MPP as

$$P_f = \frac{1}{2}-\frac{1}{\boldsymbol{p}}\int_0^\infty \sin(\boldsymbol{b}t +\frac{1}{2}\sum_{i=1}^{n-1}\tan^{-1}(-\boldsymbol{k}_i t))\frac{\exp[-\frac{1}{2}t^2]}{t[\prod_{i=1}^{n-1}(1+\boldsymbol{k}_i^2 t^2)]^{1/4}}dt \tag{1.5}$$

Der Kiureghian et al. [23] presented a second-order approximation method based on paraboloid approximation fitting around the most probable point. In another paper, Der Kiureghian [24] developed an efficient algorithm to determine the principal curvature in an iterative manner for second order structural reliability analysis.

Koyluoglu et al. [25] proposed a closed form second-order approach for reliability estimation. It has been revealed that their algorithm can yield accurate

results even for small or negative b values. Zhao and Ono [26] described a SORM procedure in which they first give a simple approximation, then present an empirical second-order reliability index to estimate the probability of failure, and finally evaluate the probability of failure using the Inverse Fast Fourier Transformation. Hohenbichler et al. [27] reviewed the classical FORM and SORM and advanced a set of asymptotic formula that can be used in computing the probability of failure for systems that can be modeled as intersections or unions.

Even though in general, simulation or analytical techniques work very well for most problems, they could encounter computational difficulty when the limit state function is not an explicit function of random variables but has to be determined using a complicated structural analysis procedure. In this case, Response Surface Methodology (RSM) has been used to obtain an analytical approximation of the implicit limit state function, which is then used in combination with FORM/SORM or other approaches to estimate the structural reliability. RSM has been proven to be a good approach for complex structural systems and those involving complicated limit state functions [28-31].

Besides the approaches mentioned, artificial intelligence technique has emerged as a potential tool for structural reliability analysis. Shao and Murotsu [32] suggested an approximate limit state function using neutral networks and they also developed an active learning algorithm which makes it possible for the neutral network to actively search the critical failure region.

1.3 Review of Literature on Manufacturability-Based and Reliability-Based Optimization

Rais-Rohani [10] proposed a three-tier strategy that examines factors such as complexity, compatibility, and efficiency in a pre-optimization stage in order to develop a manufacturability index based on material type / form and the primary manufacturing process. The design concept with the highest manufacturability index is then optimized based on performance and cost constraints [33]. Fenyes [34] used forming strain and elastic recovery (i.e., springback) to introduce formability constraints in design optimization of structural parts produced by the stamping process. Martinez et al. [35] used manufacturing cost, weight, and structural deflection as multiple objectives to be optimized using the physical programming method.

For reliability-based optimization, Frangopol [36] presented a sensitivity analysis technique that was later applied to design optimization of a redundant structure in which weight was taken as the objective function while a prescribed reliability was taken as constraint. Fu and Frangopol [37] developed a vector–optimization approach for structural design problems when multiple, often conflicting, requirements on limit states are considered simultaneously, and they also suggested a three-step reliability-based vector–optimization search strategy in the solution of the optimization problem.

Yang and Nikolaidis [38] performed a system reliability-based optimization for an aircraft wing subjected to gust loads in which FORM was employed to calculate reliability indices of various components while Ditlevsen bound technique was adopted to obtain the system reliability index. A two-level optimization problem, in

which weight was taken as objective function and system reliability was treated as a constraint, was presented by Yang and Ma [39] for composite structural systems.

Enevoldsen and Sorensen [19] have suggested four different procedures to solve the reliability-based optimization of series systems of parallel systems. Among them the first two are sensitivity based approaches and the last two are sequential methods including constant objective function method (COFM) and bounds iteration method (BIM), in which BIM has been shown to be fast and stable for an illustrating example. In another paper by the same authors [40], many aspects associated with reliability-based optimization in structural engineering have been discussed. A variety of reliability–based optimization problems were formulated and FORM was employed to estimate reliability at both component and system levels, and a two-level strategy was suggested to solve the reliability-based optimization. The selection of first-order optimization algorithms in conjunction with an efficient sensitivity analysis tool enhanced the performance of the reliability-based optimization. They also extended their discussion by examining several practical issues in reliability-based optimization including the use of finite element analysis. They concluded the discussion by the description of a strategy for model correction and refinement in model and optimal result evaluation.

Royset and Der Kiureghian [41] presented a decoupling approach by which the optimization problem can be reformulated into a deterministic, semi-infinite optimization problem (characterized by a finite number of design variables and an "infinite" number of constraints). This approach was then applied to reliability-based optimization of series structural systems with two optimization formulations. In one,

cost was minimized under the reliability and structural constraints while in the other the reliability was treated as the objective function subject to cost and structural constraints. The advantage of this approach lies in the flexibility that any optimization algorithm for semi-infinite programming and any reliability method can be adopted independently for the solution of reliability-based optimization since the optimization and reliability calculations are totally decoupled.

Analytical techniques, mainly FORM/SORM will always be a good choice for assessment of component reliability in reliability-based optimization problems when analytical model of limit state function or an equivalent approximation is available.

A one-level optimization strategy suggested by Kuschel and Rackwitz [42] based on FORM using optimality criteria was employed to solve the two formulations of reliability-based optimization problem. The first optimized cost with reliability constraints while the second optimized reliability under cost constraints. For both of them, the costs are the sum of initial cost plus the failure cost, which is estimated as the product of the cost caused by failure multiplied by the probability of failure. The algorithm was illustrated by three examples, and the optimization results were compared to those obtained by other available optimization methods in the literature in terms of computational effort involved. One disadvantage of the algorithm is that it is limited to only one limit state function, so it is not applicable to system reliability-based optimization problems.

Feng and Moses [43] performed a structural optimization treating probability of failure of the whole system as a constraint. An optimality criterion was used to solve the optimization problem.

For reliability-based optimization, two approaches, including conventional reliability index and target performance approach, were used to determine the satisfaction of constraints on structural reliability. Lee et al. [44] made a comparative study, and found that the target performance approach was computationally more efficient and robust than conventional reliability index approach for the example problems considered.

Wang and Grandhi [45] established a set of methodologies that have applications in system reliability-based optimization problems. For the purpose of accurate and efficient estimation of the probability of failure for highly nonlinear limit state functions, they proposed a higher-order reliability method (HORM) to calculate the probability of failure based on the estimated reliability index obtained from an efficient safety index algorithm. Ditlevsen upper bound was then employed to compute the system reliability for which the joint points are located using a faster algorithm using a higher order approximation. The two-point nonlinear approximation was developed to conduct the system reliability-based optimization. The advantage of their approach was demonstrated by numerical test examples.

Frangopol and Maute [46] recently presented a brief review of the life-cycle reliability-based optimization methods and their applications in civil and aerospace structures with attention to the most important approaches and recent developments. Their list of references provided a collection of the relevant problems in reliability-based optimization.

Papadrakakils and Lagaros [47] presented a methodology for reliability-based optimization for which MCS with importance sampling was adopted to assess the reliability while neutral network was used to perform the optimization.

The application of RSM in computing the reliability for reliability-based optimization can be seen in the paper of Gasser and Schueller [48], and that of Su et al. [49].

In this thesis the analytical reliability estimation technique (FORM) is used for component reliability analysis. We chose FORM because its efficiency makes it very suitable for reliability-based optimization.

1.4 Scope of Present Work

The successful design of an aircraft structure is measured not only in terms of its capacity to support the required loads but also based on many additional requirements that include efficiency, safety, producibility, and affordability. These requirements when considered together form a coupled set of multidisciplinary constraints often with conflicting demands on the structure. In addition to these requirements, if the structure is expected to be of high quality, then it must also be robust in presence of uncontrolled variations in material properties as well as geometric dimensions (tolerance) that are commonly encountered during the process of manufacturing the structure.

To properly address the influence of parametric, modeling, and other uncertainties in the design process, we must employ non-deterministic design methods where inherent and statistical variations can be adequately modeled.

In this thesis, we present a framework for probabilistic design optimization of aircraft structures where requirements for reliability, manufacturability, and cost are introduced as design constraints. The described procedure is then applied to the design optimization of a built-up wing spar where the structural sizing and applied load parameters as well as the material properties are treated as probabilistic random variables.

The objectives of this thesis are as follows:

- Discuss the framework for probabilistic design optimization with a multidisciplinary set of constraints.

- Present the metrics-based techniques for producibility analysis and cost estimation.

- Apply the design methodology to an aircraft structures problem.

- Examine the effects of manufacturability, reliability, and cost constraints on structural design.

- Compare shear-resistant web design concept with one based on diagonal semi-tension field concept.

- Present probabilistic design sensitivities associated with each component reliability.

- Discuss trade-offs among weight, reliability, and cost in the optimization results.

This thesis has been organized into seven chapters. Following an introduction in Chapter I, Chapter II describes the basic concepts underlying reliability index evaluation with focus on FORM. The advantages and disadvantages of several MPP search algorithms are discussed. Chapter III presents the MC/DG approach for the manufacturing cost estimation. Chapter

IV formulates a multidisciplinary optimization program with the primary steps and important equations highlighted. Chapter V provides brief description of developed computer program. The optimization results are presented and discussed in Chapter VI. Chapter VII presents an approach to evaluate system reliability index, which is later used to perform a system reliability-based optimization. Finally, Chapter VIII gives the conclusions for the present work and some thoughts for future work.

CHAPTER II

STRUCTURAL RELIABILITY ANALYSIS

2.1 Time-Invariant Component Reliability Analysis

The probability of failure of a structural element is generally expressed as

$$P_f = P(g(X) \leq 0) \tag{2.1}$$

where $X = \{X_1, X_2, ..., X_n\}^T$ is the vector of n random variables and $g(X)$ is the limit state function describing the failure criterion such that $g < 0$ represents failure, $g > 0$ represents safety, and $g = 0$ represents the limit state surface separating the safe and failed regions. The failure probability is found by evaluating the multiple integral of the joint probability density function $f_X(x)$ over the failure region, Ω as

$$P_f = \int \int ... \int_\Omega f_X(x_1, x_2, ..., x_n) dx_1 dx_2 ... dx_n \tag{2.2}$$

For problems involving multiple random variables, the integration of $f_X(x)$ is in general very difficult. Hence, the probability of failure is estimated using a variety of techniques including those commonly known as the random sampling methods (e.g., Monte Carlo simulation), analytical methods (e.g., First Order Reliability Method, FORM [50]), or hybrid methods (e.g., AMV+ combined with AIS [51]).

In applying the analytical or fast probability integration methods, the limit state $g(X) = 0$ is transformed to $g(u) = 0$ where u is the vector of standardized, independent

16

normal variables. Then MPP, the point on $g(\boldsymbol{u}) = 0$ where the joint probability density

function is maximum, is found by solving the following optimization problem

$$\text{Minimize} \qquad D = \sqrt{u^T u}$$

$$\text{Such that} \qquad g(\boldsymbol{u}) = 0 \qquad\qquad (2.3)$$

where D represents the distance from the origin of the transformed coordinate system

to MPP at $\boldsymbol{u}^*$ commonly referred to as the reliability or safety index, $\boldsymbol{b}$.

The optimization problem in Equation (2.3) may be solved using a variety of

mathematical programming techniques [13] or other tailor-made techniques including

those developed by Hasofer and Lind [15] and extended by Rackwitz and Fiessler

[16] to problems involving non-normal random variables.

Using the advanced first-order second-moment method proposed by Rackwitz

and Fiessler, each random variable is transformed from the original to the standard

normal space according to the formula

$$u_i = \frac{x_i - \boldsymbol{m}_{X_i}^N}{\tilde{\boldsymbol{s}}_{X_i}^N}, \qquad i = 1, 2, ..., n \qquad\qquad (2.4)$$

where $\boldsymbol{m}_{X_i}^N$ and $\tilde{\boldsymbol{s}}_{X_i}^N$ represent the equivalent normal mean and standard deviation,

respectively, and are found by matching the cumulative distribution function (CDF)

and the probability density function (PDF) of the original and equivalent standard

normal variable at the design point $\boldsymbol{x}^*$ and rearranging the resulting expressions to

find

$$\boldsymbol{m}_{X_i}^N = x_i^* - \tilde{\boldsymbol{s}}_{X_i}^N \Phi^{-1} \left[F_{X_i}(x_i^*) \right] \qquad\qquad (2.5)$$

$$\tilde{\boldsymbol{s}}_{X_i}^N = \frac{\boldsymbol{f}\left\{ \Phi^{-1} \left[F_{X_i}(x_i^*) \right] \right\}}{f_{X_i}(x_i^*)} \qquad\qquad (2.6)$$

where f_{X_i} and F_{X_i} are the PDF and CDF of X_i, while f and Φ are the PDF and CDF of u_i, respectively.

The location of MPP and the corresponding reliability index are found through an iterative solution based on an initial guess of MPP location with a local approximation of $g(u)$ at MPP for estimating the probability of failure. The accuracy of the probability of failure, thus, depends on the accuracy of the approximate limit state function. If the limit state is approximated by a linear function as

$$g(\boldsymbol{u}) = a_0 + \sum_{i=1}^{n} a_i(u_i - u_i^*) \tag{2.7}$$

then the probability of failure is estimated using the relationship $P_f \approx \Phi(-\boldsymbol{b})$.

Currently, There are several iterative algorithms that can be used for the solution of Equation (2.3). The basic idea behind them is to find MPP according to an iterative procedure, which is given by,

$$u_{k+1} = u_k + ds_k \tag{2.8}$$

where k is the iteration number and s is a vector search direction in the design space. The scalar quantity d defines the distance, usually called step length, which we wish to move in direction s_k [52].

Among all available algorithms, HL-RF algorithm is the most efficient and widely used method [53]. This method is based on the following recursive formula

$$s_{k+1} = \frac{1}{\left|\nabla g(u_k)\right|^2}[\nabla g(u_K)y_k - g(u_k)]\nabla g(u_K)^T - u_k \qquad (2.9)$$

where $\nabla g(u_K)$ is the gradient vector of the limit state function, and the step length d equals unity.

Compared with other algorithms, HL-RF algorithm is very efficient, but its convergence cannot be always guaranteed [53-54]. In order to improve the robustness of HL-RF algorithm, a merit function constructed by Liu and Der Kiureghian [54] as

$$m(u) = \frac{1}{2}\left|u - \frac{\nabla g(u_K)u}{\left|\nabla g(u_k)\right|^2}\nabla g(u_K)\right|^2 + \frac{1}{2}cg(u)^2 \qquad (2.10)$$

was introduced to guide the selection of step length such that $m(u_{k+1}) < m(u_k)$ instead of keeping it at unity as in the original HL-RF algorithm. In equation (2.10), c is a positive constant. As demonstrated by Liu and Der Kiureghian [54], the robustness of original HL-RF is greatly improved after this modification. However, the global convergence of the modified algorithm is still not guaranteed.

Sequential Quadratic Programming (SQP) was noted as the most efficient and robust method for nonlinear finite element reliability analysis and it is globally convergent under mild condition [54]. However, as noted by Abdo and Rackwitz [55], the SQP will become less efficient and less reliable than other gradient based algorithms for large number of random variables.

A global convergent algorithm based on HL-RF algorithm enhanced by step length update was due to Abdo and Rackwitz [55] and was found superior to the original HL-RF algorithm in any dimension and superior to SQP in larger dimension.

2.2 Reliability Sensitivity Analysis

Sensitivity analysis is employed to provide information about the influence of each random variable and its uncertainty on the failure probability or the reliability index, $\boldsymbol{b}$. The sensitivity factors representing the probabilistic sensitivity derivatives of $\boldsymbol{b}$ with respect to the mean value and standard deviation of random variable X_i are calculated at the design point designated by x^* as [53]

$$\left.\frac{\partial \boldsymbol{b}}{\partial \boldsymbol{m}_{X_i}}\right|_{\boldsymbol{x}^*} = \left(\frac{\partial \boldsymbol{b}}{\partial u_i}\right)^* \left(\frac{\partial u_i}{\partial \boldsymbol{m}_{X_i}}\right)^* \tag{2.11-a}$$

$$\left.\frac{\partial \boldsymbol{b}}{\partial \tilde{\boldsymbol{s}}_{X_i}}\right|_{\boldsymbol{x}^*} = \left(\frac{\partial \boldsymbol{b}}{\partial u_i}\right)^* \left(\frac{\partial u_i}{\partial \tilde{\boldsymbol{s}}_{X_i}}\right)^* \tag{2.11-b}$$

where the first partial derivative in the right hand side represents the direction cosine with respect to u_i evaluated as

$$\boldsymbol{a}_i^* = \frac{\left.\dfrac{\partial g}{\partial X_i}\right|_* \tilde{\boldsymbol{s}}_{X_i}^N}{\sqrt{\displaystyle\sum_{i=1}^{n}\left(\left.\dfrac{\partial g}{\partial X_i}\right|_* \tilde{\boldsymbol{s}}_{X_i}^N\right)^2}} \tag{2.12}$$

While the sensitivity factors in Equation (2.11-a) can help measure the influence of each random variable on $\boldsymbol{b}$, those in Equation (2.11-b) quantify the effect of parametric uncertainty on component reliability.

CHAPTER III

MANUFACTURING COST ESTIMATION

In an effort to facilitate the consideration of manufacturing cost in early stages of aircraft structural design, the Air Force Wright Aeronautical Laboratories initiated a program in the late 1970's to develop what became known as the Manufacturing Cost / Design Guide (MC/DG). That program involved a coalition of several aerospace companies, which at the time included such companies as the Grumman Aerospace Corporation, Lockheed-California Company, and Northrop Corporation.

A series of reports were published by the Battelle's Columbus Laboratories, which acted as the principal contractor in that effort. Those reports provided useful information related to the cost-driver elements (CDE), cost-estimating data (CED), and relative recurring and nonrecurring tooling cost estimates for the manufacture of discrete aerospace parts as well as for mechanically fastened structures. The cost estimation models used here are based on the information contained in some of the MC/DG reports [56-59].

Similar to MC/DG, The total manufacturing cost is calculated here as the sum of recurring and nonrecurring costs measured in units of labor hours. The recurring labor costs include those associated with the manufacture of individual discrete parts, mechanical assembly of the parts into a built-up structure, as well as testing, inspection, and evaluation (TI&E) of the assembly and its individual parts.

Furthermore, the additional cost penalty as a result of increased manufacturing complexity over the baseline design is also included in recurring cost estimations. According to MC/DG the so-called Designer-Influenced Cost Elements (DICE) are those manufacturing complexities that require either additional standard manufacturing operations (e.g., joggles, flanged holes, and beads) or special shop operations (e.g., heat treatment, special tolerances, and special finish).

Although the recurring cost of a discrete part usually includes the cost of raw materials as well as the manufacturing labor cost, we decided to exclude the raw material cost since we are not making any comparison between different material systems.

The nonrecurring cost consists of the tooling cost as well as the testing, inspection, and evaluation cost. Therefore, the general equation for manufacturing cost of a discrete part (DPC) can be expressed in terms of its direct recurring cost (*PRC*) and nonrecurring cost (*PNRC*) as

$$DPC = PRC + PNRC \tag{3.1}$$

$$PRC = (RC_p + DICE_p + RC_{TI\&E} + DICE_{TI\&E})LCF_P \tag{3.2-a}$$

$$PNRC = NRC_T + NRC_{TI\&E} \tag{3.2-b}$$

which includes the recurring labor cost (RC) of manufacturing the base part, RC_p; the additional labor cost of manufacture due to DICE, $DICE_p$; the RC for TI&E of the

base part, $RC_{TI\&E}$; the additional labor cost of TI&E due to DICE, $DICE_{TI\&E}$; the learning curve factor for part manufacture, LCF_P; the nonrecurring tooling cost, NRC_T; and the nonrecurring TI&E cost, $NRC_{TI\&E}$. All cost terms are presented in units of labor-hours.

Depending upon the part geometry and manufacturing process, separate equations are generated and used for the calculation of RC values. For example in the case of end milling, MC/DG [58] provides multiple curves (designated as CED-M/C-25) to estimate the recurring cost at unit 200 based on 80% rough and 20% finish machining operation. Each curve is designated by the initial material weight and it relates the recurring milling cost to the weight of material removed. We have used these curves to generate several analytical equations, which can be used to calculate the machining cost based on the initial material weight and the weight of material removed. For instance, if the initial weight is less than 100 lb, then the RC for milling is calculated as

$$RC = 38\,\frac{W_r}{100} \tag{3.3}$$

and if the initial weight is between 100 to 200 lb, the equation changes to

$$RC = \left[0.245\left(W_i - 100\right) + 38\right]\frac{W_r}{W_i} \tag{3.4}$$

where W_I and W_r is the initial and removed material weight, respectively. In MC/DG, the recurring cost estimates are all based on the cost at unit 200. Therefore, to obtain the cumulative average cost for the design quantity and learning curve rate considered in each case, the 200th-unit cost is multiplied by the learning curve factor, LCF found as

$$LCF = \frac{\frac{1}{P(m+1)}\left[(P+0.5)^{m+1} - (0.5)^{m+1}\right]}{200^m} \tag{3.5}$$

where P is the design quantity produced, and $m = \ln(lc)/\ln(2)$. The learning curve rate, lc, which for sheet metal forming, conventional machining, and bench-top assembly is assumed to be 90%, 80%, and 85%, respectively [58].

Similar to Equation (3.1), the total assembly cost, TAC is found as

$$TAC = ARC + ANRC \tag{3.6}$$

where ARC is the recurring assembly cost similar to Equation (3.2-a), and is affected by the total number of fasteners in assembly, method of fastener installation (e.g., manual, automatic, or combination), and whether the installation is dry or requires sealant [59]. In this case, the assembly learning curve factor, LCF_A depends on the design quantity, and the learning curve rate associated with a particular method of assembly (e.g., bench top, floor, or final). The nonrecurring assembly cost, $ANRC$ is found using Equation (3.2-b) by replacing the part cost data with that of the assembly [57]. Thus, the total manufacturing cost for a built-up structure is obtained as

$$TMC = \sum_{i=1}^{NDP} DPC_i(PPS_i) + TAC \tag{3.7}$$

where DPC_i is the manufacturing cost of the ith discrete part, PPS_i is the quantity of ith discrete parts used in the assembly, and NDP is the number of discrete parts.

Although not exact, these cost estimates render a meaningful economic scale by which different design concepts can be compared in terms of relative manufacturing cost.

CHAPTER IV

WING SPAR DESIGN OPTIMIZATION PROBLEM

4.1 Product and Process information

A wing spar is modeled as a tapered cantilever beam (shown in Figure 4.1) supporting a uniformly distributed force along length d, which then decreases linearly to zero at the tip. We are assuming this load to represent the design ultimate load in this problem.

The spar height decreases linearly from root to tip such that $H_2 = 0.5\ H_1$. The spar structure consists of a flat web supported by an upper and a lower cap as well as a series of web stiffeners distributed along its length. The spar web is made up of three flat sheets (Segments 1-3) of equal length that are spliced together at two joints located at $L/3$ and $2L/3$ as shown in Figure 4.1. The absolute minimum number of web stiffeners is 4 with one placed at each spar end and one at each web splice location as shown in Figure 4.2. All parts in the assembly are mechanically fastened with the same type fasteners.

The one-piece upper and lower spar caps are machined extrusions with identical cross-sectional shape and size as shown in Figure 4.3. While preserving the cross-sectional symmetry, the thickness and width of horizontal flanges are allowed to decrease linearly from the root to tip according to the specified taper ratio, TR, such

that $(w_{1tip}, t_{1tip}) = TR(t_1, w_1)$. By contrast, the thickness and width of the vertical flange (t_2, w_2) are kept uniform along the length. The learning curve for machining is in the range of 80% (conventional) to 95% (computer numerical controlled) with the average value used in calculation of the caps' recurring labor cost

Each of the three web segments has a uniform thickness, which can be different from the other two. The web stiffeners are extruded angle sections with identical flanges as shown in Figure 4.3. These stiffeners are identical in cross-sectional dimensions and only different in length. The web stiffeners are not machined.
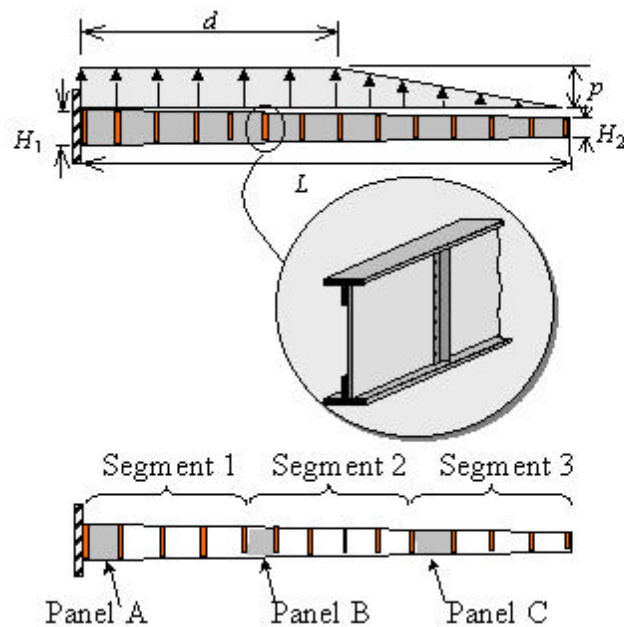
Figure 4.1: Spar geometry and loading condition
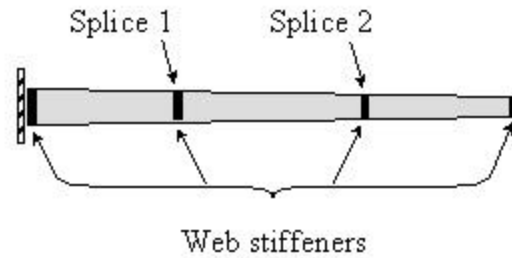
Figure 4.2: Spar geometry with absolute minimum number of web stiffeners
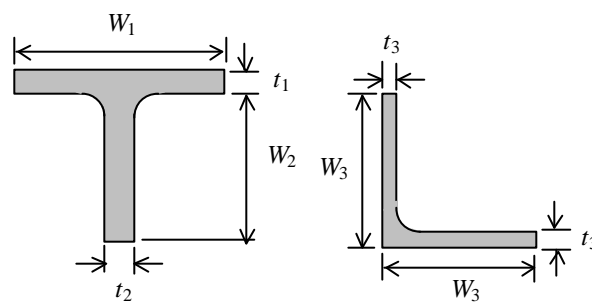
Figure 4.3: Cross-sectional geometry of the spar caps with dimensions at the root section (a) and web stiffeners (b)

The two different design concepts considered in this example problem are as follows:

- Concept 1: The web is in the state of pure shear limited in resistance by the shear buckling strength in each web panel

- Concept 2: The web is allowed to go beyond buckling into diagonal semi-tension field

Because of this contrast, the failure modes in the two concepts are distinctly different.

Table 4.1 describes the material type, material form, and the primary manufacturing process used to produce each spar part. The table also defines the

method of assembly as well as the type of fasteners used. The total number of spars to be produced is assumed to be 50.

Table 4.2 provides the listing of random variables (RVs) and corresponding statistical properties. All RVs are assumed to be statistically independent and normally distributed with the first 8, which represent the cross-sectional dimensions of the spar caps at the root, stiffener flange dimensions, web thickness in Segment 1, as well as the taper ratio (see Figure 4.1), making up the vector of design variables. The spar length and height dimensions, which are ordinarily defined by the wing aerodynamic shape, are excluded from the vector of design variables.

The reliability index depends on the mean, standard deviation as well as the distribution type of each random variable. When a structural dimension with bilateral tolerance is treated as a random variable, then it is possible to relate its standard deviation to the tolerance range using the following relationship [61]

$$\tilde{s}_X = \frac{\Delta_u + \Delta_l}{F} \quad (\text{for } X^{+\Delta_u}_{-\Delta_l}) \tag{4.1}$$

where F is a factor that depends on NP, the number of parts produced. For example, if $NP = 25$, then $F = 4$ whereas for $NP = 100$, $F = 5$. Equation (4.1) provides a means for capturing dimensional uncertainty and establishing a correlation between structural reliability and the manufacturing process as the natural tolerances are governed by the capability of the manufacturing process used.

Table 4.1: Wing-spar parts and process specifications

Cap Design: Tee section	
Material type	2024-T3[a]
Material form	Extrusion
Final thickness	Variable
Primary process	End Milling[b]
lc	80 - 95%
Web Design: Flat sheet	
Material type	2024-T3
Material form	Sheet
No. of segments	3
Splice type	Doubler
Primary process	Shearing
lc	90%
Stiffener Design: Angle section	
Material type	2024-T3
Material form	Extrusion
End joggles	None
Primary process	Cutting ends
lc	90%
Fastener Design: Flat-head	
Material type	2017-T3
Web-Cap	1/4 in. dia., 2 rows
Web-Stiffener	3/16 in. dia., 1 row
Sealant	None (Dry)
Assembly: Bench-top	
Method	100% manual
lc	85%
Prod. quantity	50

[a] Initial heat treatment prior to machining
[b] Includes 80% rough and 20% finish machining

Table 4.2: Description of independent random variables

RV No.	RV Definition	Mean Value	Standard Deviation
1[a]	W_1, in.	Y_1	0.001
2[a]	t_1, in.	Y_2	0.001
3[a]	W_2, in.	Y_3	0.001
4[a]	t_2, in.	Y_4	0.001
5[a]	W_3, in.	Y_5	$0.01Y_5$
6[a]	t_3, in.	Y_6	$0.01Y_6$
7[a]	t_{web}, in.	Y_7	0.002
8[a]	TR	Y_8	$0.01Y_8$
9	H_1, in.	12	0.10
10	L, in.	216	0.12
11	d, in.	144	43.2
12	p, lb/in.	33.33	10.0
	2024-T3 Extrusion		
13	Young's Modulus, psi	10.8×10^6	0.54×10^6
14	T. Yield Stress, psi	51×10^3	2.60×10^3
15	C. Yield Stress, psi	42×10^3	1.73×10^3
	2024-T3 Bare Sheet		
16	Young's Modulus, psi	10.5×10^6	0.525×10^6
17	Poisson's ratio	0.33	0.0165
18	T. Yield Stress, psi	49.3×10^3	0.86×10^3

[a] Design variables

For the spar caps, the specified tolerance is defined by the vertical (end) milling process [62] (i.e., $\Delta = \pm 0.0025$ in.). Considering the total number of spar caps produced at 100 (i.e., $F = 5$), we obtain the standard deviation values for design variables 1 through 4 as shown in Table 4.2. For the extruded parts that do not require any machining operation (i.e., the stiffeners) the allowable tolerances for flange thickness and width are specified as $\pm 2.5\%$ of wall thickness and flange width, respectively [63]. Using the specified tolerance and $F = 5$, the standard deviation values for design variables 5 and 6 are found to be 0.01 times the mean wall thickness and flange width, respectively. The standard deviation for the web thickness, design variable 7, is based on the sheet thickness tolerance of ± 0.005 [61]. For the taper ratio, we assumed a coefficient of variation of 10%. For the length of spar and its height at the root, which are influenced by the assembly process (assumed to be 100% manual), the tolerance is set at ± 0.25 in. resulting in the standard deviation of 0.12 and 0.1, respectively.

Since the external load is usually subject to a greater scatter, we assumed a coefficient of variation of 30% for both d and p (see Figure 4.1).

The material properties shown in Table 4.2 are obtained from MIL-HDBK-5G. In the case of Young's modulus and the Poisson's ratio, the coefficient of variation of 5% is used [64] whereas in the case of yield stress, the A- and B-basis values are used to calculate the mean and standard deviation as [61]

$$\tilde{m} = 2.32\,B - 1.32\,A \tag{4.2}$$

$$\tilde{s} = \frac{B - A}{1.158} \tag{4.3}$$

4.2 Design Optimization Formulation

The probabilistic design optimization of a structural system involving a multidisciplinary set of constraints is formulated as

$$\text{Minimize} \quad f(\mathbf{X})$$

Subject to:

$$g^d(\mathbf{X}) \le 0$$
$$g_i^m(\mathbf{X}) \le 0, \qquad i = 1, 2, ..., NM$$
$$g^c(\mathbf{X}) \le 0 \tag{4.4}$$
$$g_j^f(\mathbf{X}) \le 0, \qquad j = 1, 2, ..., NF$$

$$Y_k^l \le Y_k \le Y_k^u, \qquad k = 1, 2, ..., NDV$$

where $\mathbf{X}$ represents an n-dimensional vector of random variables with the mean values of its subset treated as design variables $(Y_k, k = 1, 2, ..., NDV)$. The design constraints are separated into four groups with g^d representing the constraint on mean displacement at the tip, g_i^m representing a vector of NM manufacturability constraints, which includes restrictions associated with the manufacture of discrete parts as well as their assembly, g^c representing the constraint on the mean value of the total manufacturing cost, and g_j^f representing a vector of NF reliability constraints. Additionally, each design variable, Y_k is bounded by the specified side constraints, Y_k^l and Y_k^u.

In the context of reliability-based design optimization, the reliability constraints are formulated either in terms of the probability of failure or reliability (safety) index

[60]. If we impose a constraint on minimum safety index as a surrogate for probability of failure, then the reliability constraints are expressed as

$$1 - \frac{b_i^f}{b_i^{f\min}} \leq 0 \tag{4.5}$$

where $b_i^{f\min}$ is the minimum value of safety index associated with failure in the ith structural member or ith failure mode.

The spar design optimization problem as defined by Equation (4.4) is solved by searching the feasible design space for the optimal vector of design variables that would minimize the mean spar-weight subject to the specified set of design constraints described next.

4.3 Displacement Constraint

The vertical displacement at the spar tip is limited to a maximum value of 8 in. or approximately 4% of spar length. The tip displacement is calculated using the unit-load method by considering only the bending contribution to the elastic strain energy stored in the spar with the resulting integral equation solved using the trapezoidal rule. In the calculation of flexural rigidity, the caps are assumed to provide the entire bending resistance while they relieve the web from bearing all the shear resistance as the spar is tapered.

4.4 Manufacturability Constraints

The original dimensions of the spar caps (prior to machining) refer to the dimensions of the extruded parts, and they must be specified such that problems with the extrusion process may be avoided.

Subramaniam and Ulrich [8] have identified eight possible failure modes in the extrusion process among which five depend on the cross-sectional geometry and dimensions of the extruded part. They use such producibility metrics as the section balance, shape factor, and form factor to establish proper relationships between cross-sectional geometry and producibility requirements. The definition of each metric follows next.

As the billet material is pushed through the die at constant speed to produce the extruded part, it is subject to the ram force with resultant acting at the centroid of the cross-sectional area and the equal and opposite drag force with resultant acting at the center of perimeter. Due to possible eccentricity of drag and ram forces, it is possible for the extrusion to bend as it exits the die. The section balance is a metric used to predict that tendency and is defined as

$$SB = \frac{\sqrt{\Delta x^2 + \Delta y^2}}{r} \qquad (4.6)$$

where the numerator defines the distance between the center of area and center of perimeter measured in terms of Δx and Δy distance along each axis while the denominator defines the radius of a minimum circumscribing circle. For simplicity, the distance measured from the centroid of area to the farthest point on the cross section is used as the radius. As the section balance becomes larger, the extrusion's tendency to bend becomes worse. Hence, based on the information provided by Balasubramaniam [65], the constraint limit is defined as $SB \leq 0.05$.

Hot shortness refers to the surface tear and roughness of the extruded part as it exits the die. It occurs when the exit temperature is too close to the solidifying temperature of the alloy. The shape factor, denoted as *SF*, is a metric used to predict

the possibility of hot shortness and is defined as the ratio of the cross-sectional perimeter to the cross-sectional area. As the shape factor grows, the chance for hot shortness increases. Thus, based on the information provided by Balasubramaniam [65], the constraint limit is defined as $SF \leq 21$.

The circumscribing circle determines the size of press required for producing the extrusion with the extrusion pressure increasing as the wall thickness is reduced. The ratio of the diameter of the circumscribing circle to the minimum wall thickness is referred to as the form factor denoted as FF [66]. The growth in the form factor results in a greater difficulty with the extrusion process. Hence, based on the information provided by Trucks [63], the constraint limit is set at $FF \leq 60$.

Therefore, six extrusion-related producibility constraints (three for caps and three for stiffeners) are included in this optimization problem.

The initial extrusion and the final machined dimensions are correlated by assuming that the optimal spar cap dimensions at the root are equal to 90% of the original extrusion dimensions. Since there is no machining involved in production of web stiffeners, there is no difference between the optimal and extruded stiffener dimensions.

In addition to constraints on manufacturability of extruded parts, there are additional constraints due to assembly requirements. For example, the cap's vertical flange has to be wide enough to accommodate the use of two adjacent fasteners at 1/4-in. diameter. According to the limits specified by Niu [67], the lower bound on dimension w_2 (see Figure 4.2) is set at $7D + CR$, where D is the rivet diameter and CR

is the corner radius, which is assumed to be equal to the weighted average of t_1 and t_2 (see Figure 4.2).

4.5 Cost Constraint

The manufacturing cost is determined according to the procedure described previously based on the data obtained from MC/DG reports [56-59]. Since the spar parts do not involve any special or additional shop operation, $DICE_p = 0$. Also, the cost associated with TI&E is usually very small and is ignored in this case. What remains are essentially the recurring and non-recurring costs associated with each discrete part plus the same for the assembly. Without focusing on any single cost element, a constraint is placed on the total manufacturing cost found from Equation (3.7).

4.6 Component Reliability Constraints

For each spar design concept, we considered the dominant mode of failure in each component and required the corresponding safety index to be larger than $b_i^{f\min}$ as defined in Eq. (21). To assure uniform reliability throughout the structure, we specified the same target reliability (i.e., $b_i^{f\min} = b_{\min}$, $i = 1, 2, ..., NF$) for all components. The description of failure modes considered in each design concept is given below.

4.6.1 Spar Design Concept 1

In Concept 1, the spar caps are assumed to carry the entire bending load, hence, the strength in each web panel between two adjacent stiffeners is limited by its elastic shear buckling strength found as

$$t_{cr} = \frac{k_s pE}{12\left(1-n^2\right)}\left(\frac{t}{b}\right)^2 \tag{4.7}$$

where k_s is the shear buckling coefficient, E is the Young's modulus, n is the elastic Poisson's ratio, t is the panel thickness, and b is the short dimension of a rectangular panel based on the average dimensions of the tapered panel. The limit state function for web failure mode is defined as

$$G_w = 1 - \frac{t}{t_{cr}} \tag{4.8}$$

where t is the average applied shear stress in the web and t_{cr} is defined as Equation (4.7).

Since the spar caps, in general, are braced along two perpendicular directions by the spar web and the wing skin, the failure of the cap in compression (i.e., the upper cap) is based on its local crippling strength, which is found using the Gerard method [68], the limit state function for this failure mode is defined as

$$G_u = 1 - \frac{s_{max}}{s_{cs}} \tag{4.9}$$

where s_{max} is the maximum compressive stress for upper cap, and s_{cs} is the crippling stress. For the lower cap, its failure is based on the tensile yield stress of the cap material , the limit state function is then defined as

$$G_l = 1 - \frac{s_{max}}{s_{ty}} \tag{4.10}$$

where s_{ty} is the tensile yield stress for lower cap.

The failure of the web stiffeners is based on the minimum moment of inertia required for a non-buckling web design [68]. The limit state function for the web stiffener is defined as

$$G_s = 1 - \frac{I_s}{I_a} \tag{4.11}$$

where I_s is the required moment of inertia for stiffener and I_a is the actual moment of inertia of stiffener. Hence, the failure of the spar structure in Concept 1 is based strictly on its static strength.

The two rows of fasteners used to attach the upper and lower caps to the spar web are spaced longitudinally according to the calculated shear flow at each cap-web joint as well as the fastener size, type, and the allowable shear stress. Because of variation in transverse shear force along the spar, the fastener spacing is allowed to change from one panel to another, but it is limited to a maximum distance of 2 inches. As for the fastener spacing in the web stiffeners, it is calculated based on the average shear stress in the web at each stiffener location and is also limited to a maximum of 2

inches. This upper limit is specified mainly because the caps as well as the stiffeners are attached to only one side of the spar web (see Figure 4.1).

Based on the identified failure modes, four separate limit state functions are formulated for Concept 1. These include one per failure in the upper cap, lower cap, web, and web stiffeners, respectively. Thus, four separate safety indices are calculated according to the procedure discussed previously. To simplify this task, only the most critical region in each member is used for the calculation of safety index. Based on the support and loading condition specified, the most critical region for all members is that near the root section.

As was mentioned earlier, only the thickness of Segment 1 (see Figure 4.1) is treated as a design variable in the optimization problem. However, for the other two web segments, the thickness is calculated by setting the ratio of critical shear stress to the average applied shear stress in the first panel of segments 2 and 3 (i.e., Panels B and C) equal to that in Panel A (see Figure 4.1).

4.6.2 Spar Design Concept 2

The web design in Concept 2 is allowed to be loaded beyond buckling into diagonal semi-tension field. The analysis procedure used here is a combination of NACA and Wagner's modified methods as discussed by Bruhn [68] and Kuhn et al. [69].

As the web buckles in shear, it continues to carry load in the form of diagonal semi-tension field with the diagonal tension factor, k defined as

$$k = \tanh\left(0.5\log_{10}\frac{t}{t_{cr}}\right) \qquad (4.12)$$

When web is in complete diagonal tension, $k = 1$, and when it is in pure shear, $k = 0$; otherwise $0 < k < 1$, and is determined using Equation (4.12). The maximum shear stress in each web panel is calculated based on NACA method [67] as

$$t_{max} = t(1 + k^2 C_1)(1 + k C_2) \tag{4.13}$$

where t is defined as in Equation (4.8), C_1 is a correction factor, which allows the diagonal tension field angle a to be less than 45°, and C_2 accounts for stress concentration due to flexibility of the spar caps. Due to taper in spar web, a is calculated based on the portion of shear carried by the web.

The allowable shear stress is calculated according to Wagner's modified method [68] as

$$t_{all} = t_{cr} + \left(s_{ty} - \frac{t_{cr}}{K_r} \right) K_r R \sin a \cos a \tag{4.14}$$

where s_{ty} is the tensile yield stress of the web material, K_r is the fastener correction factor, and R is a factor similar to C_2 and depends on the web stiffener spacing, moments of inertia of the upper and lower caps, as well as a. The limit state function for web is then defined as

$$G_w = 1 - \frac{t_{max}}{t_{all}} \tag{4.15}$$

As a result of buckling, the web panels tend to pull the spar caps closer together. This action is prevented, however, by the vertical web stiffeners, which are placed under axial compressive stress. Since the stiffeners are placed only on one side of the web, they carry an average normal stress calculated as [68]

$$s_{st} = \frac{k t \tan a}{\dfrac{A_{s_e}}{dt} + 0.5(1 - k)} \tag{4.16}$$

where d is the stiffener spacing, t is the web thickness, $\boldsymbol{t}$ is the average applied shear stress, and A_{S_e} is the effective stiffener cross-sectional area. The failure stress, $\boldsymbol{s}_{JE}$, in the web stiffeners is calculated using the Johnson-Euler formula [68], which depends on the crippling strength of the stiffener as well as its effective slenderness ratio. The limit state function for stiffer is defined as

$$G_s = 1 - \frac{\boldsymbol{s}_{st}}{\boldsymbol{s}_{JE}} \qquad (4.17)$$

The cap failure analysis requires the calculation of both primary and secondary stresses [68]. The primary stresses are due to beam flexure, which places the upper cap in compression and the lower cap in tension, as well as the compressive stress in both caps due to tension field action with magnitude depending on the value of k.

The secondary stresses in the caps are created as a result of diagonal tension pulling on the caps in the vertical direction. In this case, the caps act as continuous beams with the web stiffeners as support points and the transverse load being the vertical component of the web diagonal tensile stresses. The combination of primary and secondary stresses in the upper and lower caps causes the highest loaded point in both caps to be located at their respective bottom edges. The limit state function for upper cap is defined as

$$G_u = 1 - \frac{S_{pu} + S_{su}}{S_{cs}} \tag{4.18}$$

where S_{pu} and S_{su} is the primary and secondary stress, respectively, in the upper cap. Whereas for the lower cap, the limit state function is defined as

$$G_l = 1 - \frac{S_{pl} + S_{sl}}{S_{ty}} \tag{4.19}$$

where S_{pl} and S_{sl} is the primary and secondary stress, respectively, in the lower cap.

Besides the main structural components, fastener design is also influenced by the semi-tension field design. While the cap-web fasteners are subject to a shear load that is $(1+0.414k)$ times that in Concept 1, the stiffener-web fasteners are subject to a combination of shear and tensile stresses [68]. In this case, the fastener spacing is also limited to a maximum of 2 inches.

Similar to Concept 1, four different element failure modes are considered with a limit state function defining each criterion. The reliability index associated with each failure mode is constrained in the optimization problem based on the specified value for b_{min}.

CHAPTER V

COMPUTER PROGRAM DESCRIPTION

The FORTRAN-based deterministic code, TASPI[33] was modified extensively for incorporating uncertainties associated with geometrical and material properties as well as external loads. The revised code solves the probabilistic design optimization problem in Equation (4.4) by linking the design analyses discussed previously with the general-purpose design optimization code, DOT [70].

5.1 Main Program

The primary task of the main program is to solve the given optimization problem by repeated calls to DOT and using the results obtained from the evaluation module in each iteration. In order to do the optimization, besides the statistical data for all random variables including mean, standard deviations, and distribution types, initial values and upper and lower bounds for design variables are also needed. In addition, the minimum reliability index and the maximum cost (if a cost constraint is included) should be specified in advance. All input data are stored in an input file that can be accessed by the corresponding code in the main program. The number of design variables and the number of constraints are set in the early part of the main program for the implementation of optimization. Sequential quadratic programming is chosen

for the solution of the optimization problem. The flow chart of the main program is

shown in Figure 5.1.

Data Input
- Initial values of design variables
- Lower and upper bounds
- Random variable data
  - Mean
  - Standard deviation
  - Distribution type

Set Parameters for DOT
- Optimization method
- Number of constraints
- Number of design variables

- Evaluate obj. function
- Evaluate design constraints
- Use DOT to solve design optimization problem

Convergence?

No

Yes

STOP
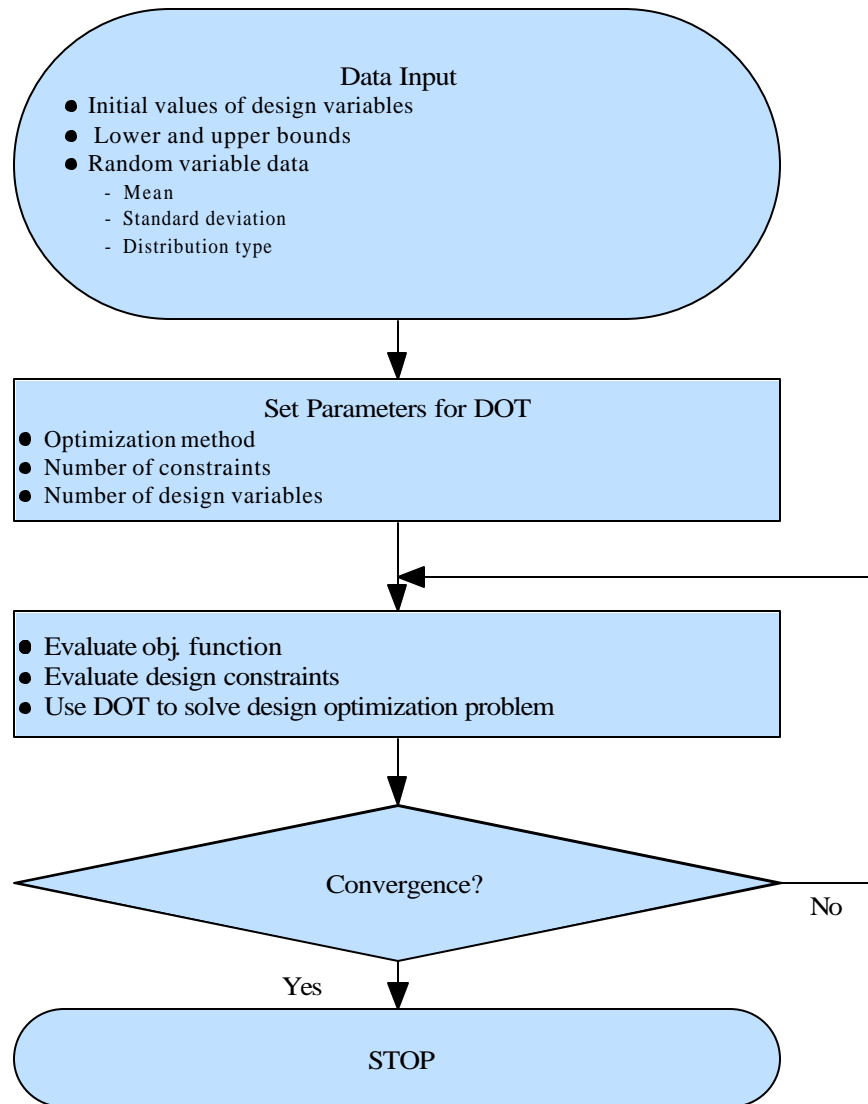
Figure 5.1: Flow chart of main program flow

5.2 Evaluations of Objective Functions and Design Constraints

The objective function is the total spar weight excluding the weight of fasteners and the material removed in drilling the corresponding holes. The calculation of weight of wing spar depends on web thickness in each segment as shown in Figure 5.2.
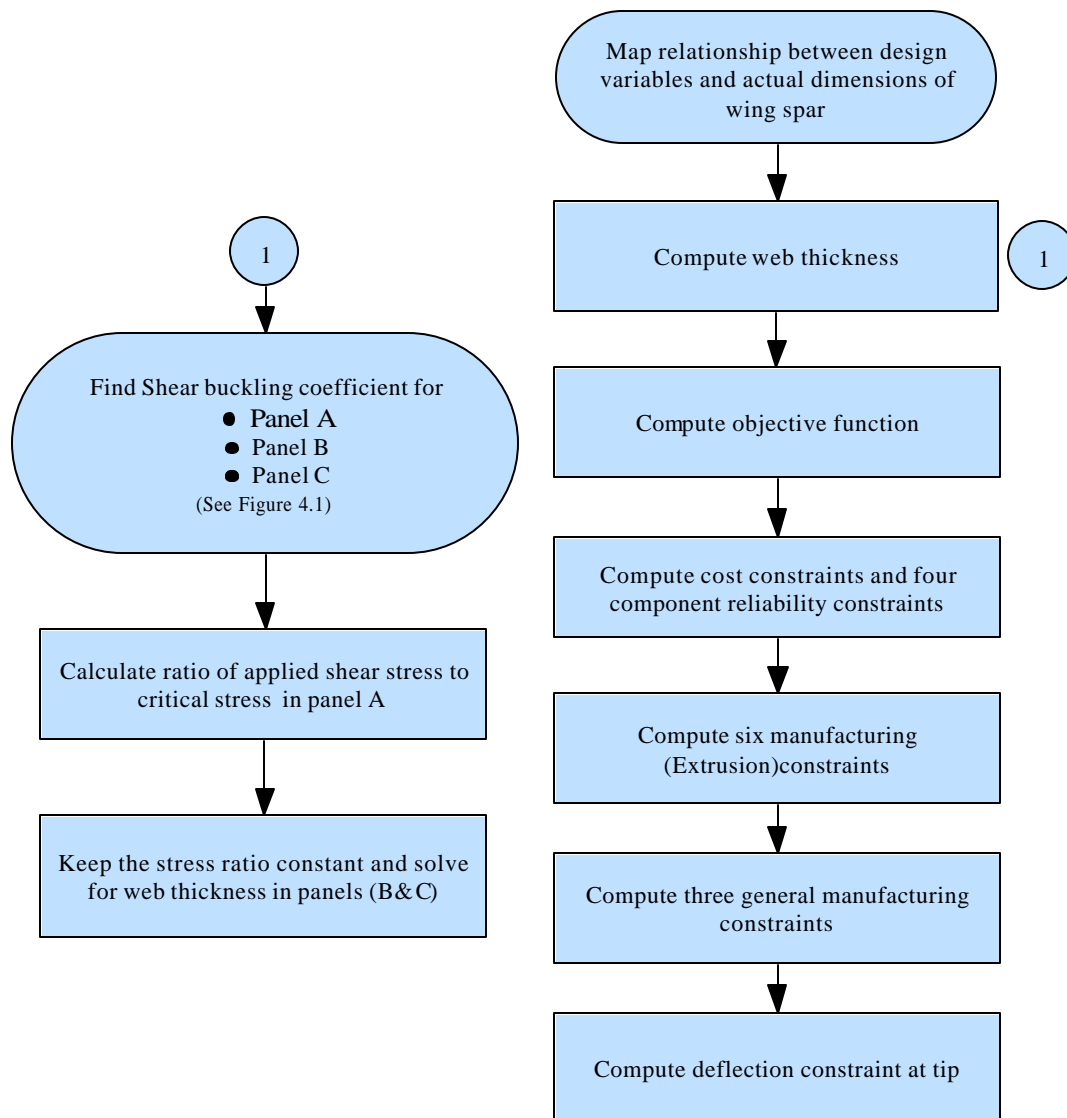
Figure 5.2: Flow chart of objective function and constraint evaluations

5.2.1 Reliability Constraints

There are totally four component failure modes for both Concepts 1 and 2. For a specified component, the limit state function in Concept 1 will be significantly different from that in Concept 2. HL-RF algorithm was employed to compute the reliability index for each failure mode for both Concepts 1 and 2, with the derivatives of limit state function with respect to random variables evaluated using the forward finite difference scheme with accurate step size. The flow chart of HL-RF algorithm applied in computing component reliability index is shown as Figure 5.3.
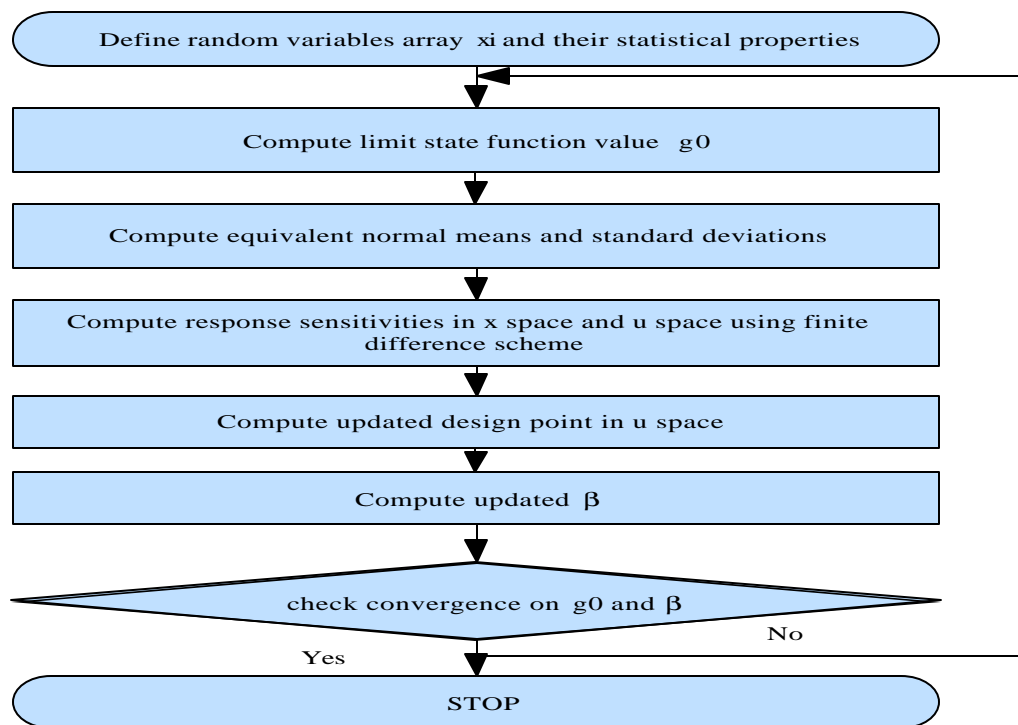
Figure 5.3: Reliability index evaluation process

5.2.2 Cost constraint

The total manufacturing cost of wing spar consists of four parts: the machining cost for the cap, shearing cost for the web, cutting cost for the stiffeners, and the assembly cost. Several subroutines were written based on MC/DG described in Chapter III. Since shearing is not covered in MC/DG, routing data was used to estimate the labor cost for shearing. For the assembly cost, the total number of fasteners should be determined. For this task, a subroutine was developed according to the discussions in section 4.61. Figure 5.4 illustrates the flow chart of this subroutine. The whole procedure for the calculation of total cost is demonstrated briefly in Figure 5.5.
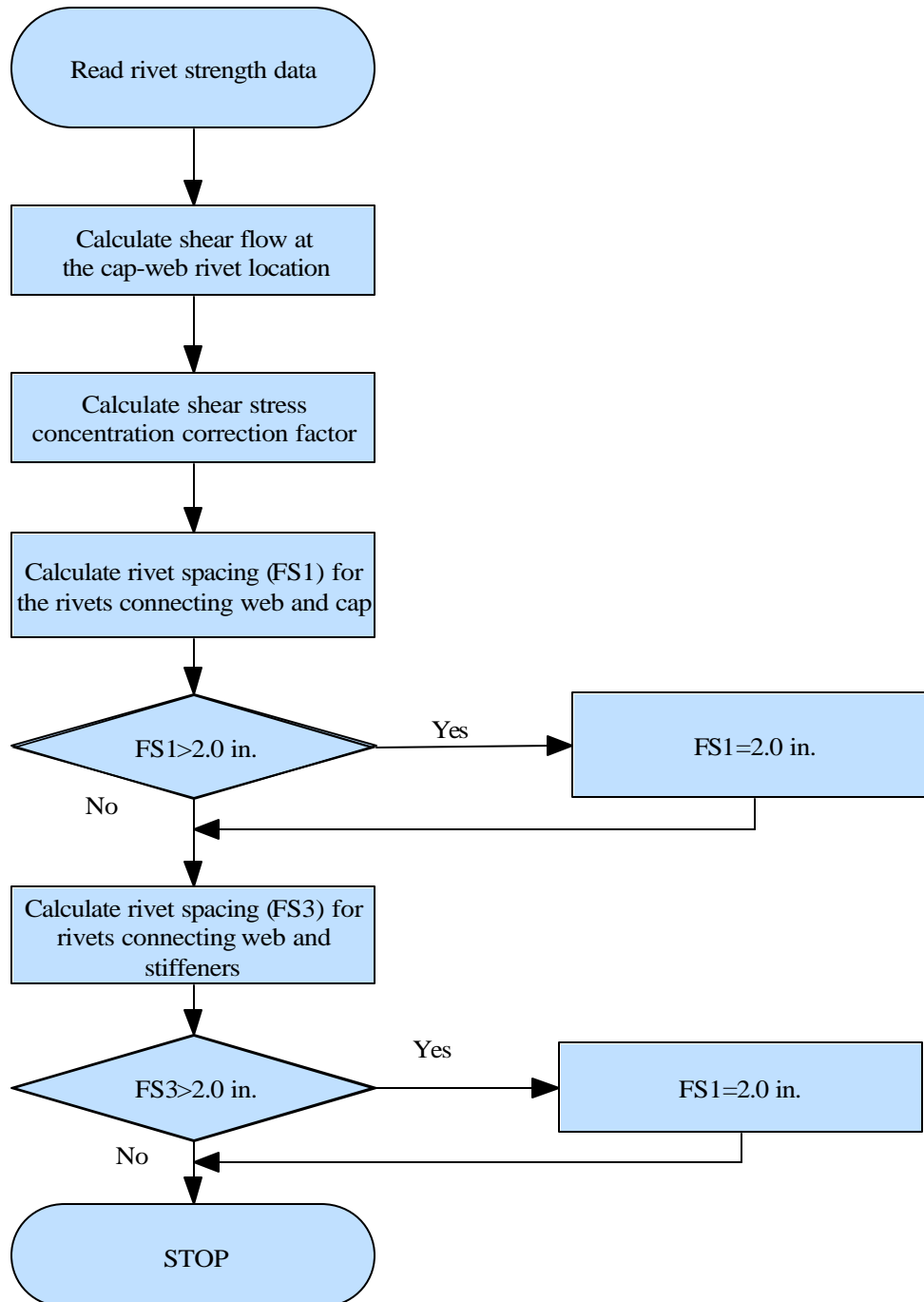
Figure 5.4: Determination of rivet spacing

Input cost information (CINPUT)

Calculate cap cost(machining)

Calculate web cost(routing)

Calculate stiffener cost(cutting)

Calculate assembly cost(assembly)

Total cost

STOP
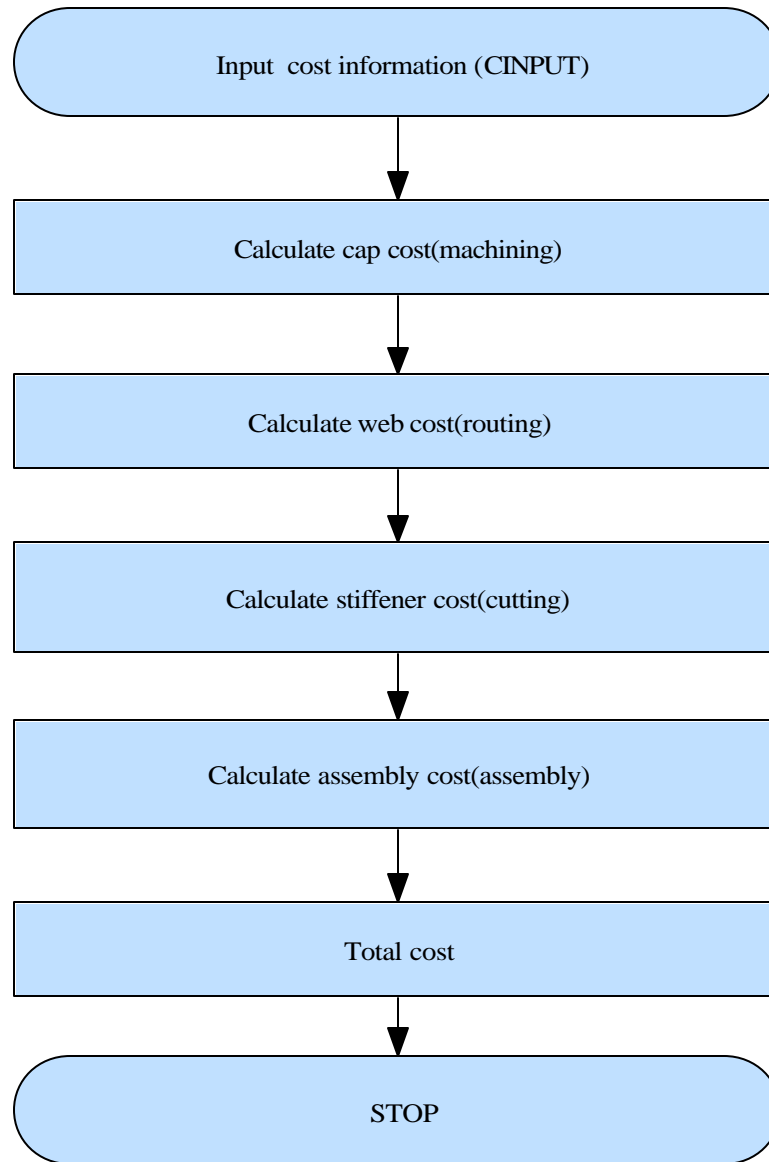
Figure 5.5: Flow Chart for the computation of total cost

5.2.3 Manufacturability Constraints

The description in section 4.4 was used to guide the development of two subroutines for the evaluation of manufacturability constraints. Three extrusion related constraints (i.e. section balance, form factor and shape factor) are imposed on the caps, and likewise the same set of extrusion constraints are needed for the stiffeners. The procedure to compute the six constraints can be seen in Figure 5.6. Besides the six extrusion related constraints, assembly constraints have also been imposed. There are three assembly constraints for Concept 1 and four for Concept 2. The procedure for evaluation of assembly constraints is implemented in another subroutine.
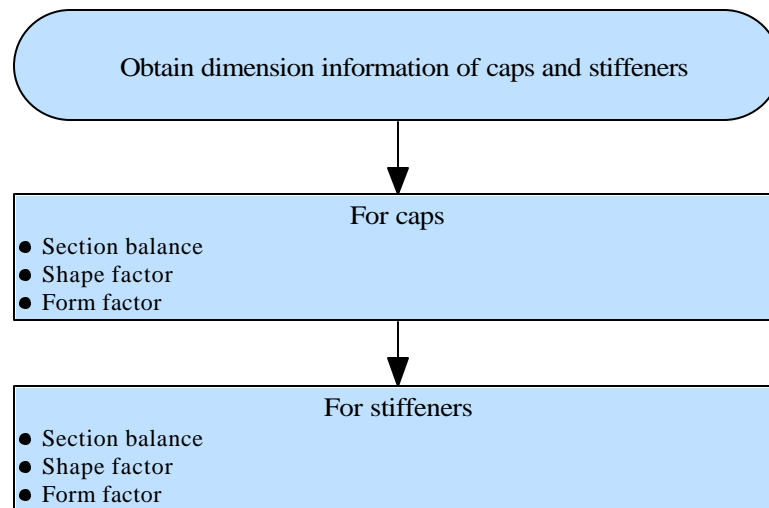
Figure 5.6: Manufacturability evaluation flow chart

CHAPTER VI

RESULTS AND DISCUSSION

The computer code described briefly in Chapter V was used to obtain the results presented here. These results reveal the influence of web design concept as well as the effects of reliability, manufacturability, and cost constraints on the optimal design. Of particular interest is the examination of relationships and trade-offs among weight, cost, and reliability.

6.1 Spar Design Concept 1

The solution depends on the number and location of web stiffeners. Besides the four stiffeners shown in Figure 4.2, additional stiffeners are placed incrementally until an optimum solution is found without any design constraint violation. Figure 6.1 shows the distribution of the seven web stiffeners found to be the minimum feasible number for Concept 1. Segment 1 has two evenly spaced intermediate stiffeners (3 panels), Segment 2 has one stiffener in the middle (2 panels) while Segment 3 has none (1 panel).

Segment 1   Segment 2   Segment 3
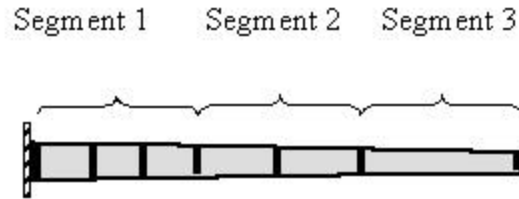
Figure 6.1 Distribution of the minimum feasible number of web stiffeners for Concept 1

The optimization results for Concept 1 are shown in Table 6.1. All component reliability indices are constrained to have the same minimum with selected values shown in column 1 of Table 6.1. To examine the effect of target reliability index, four different values of b_{min} are tested. Also to investigate the influence of cost constraint, the optimization problem is solved first without any limit on cost, then solved again by requiring the total manufacturing cost to be less than 90% of the cost found in the previous optimization problem.

For each value of b_{min}, the standard deviation for spar weight is obtained by calculating the partial derivative of weight with respect to each independent random variable and using the formula

$$\tilde{s}_W = \sqrt{\sum_{i=1}^{n} \left(\frac{\partial W}{\partial X_i}\right)^2 \tilde{s}_{\tilde{X}_i}^2} \qquad (6.1)$$

where W represents the total spar weight. The same formula is used for the calculation of standard deviation for cost by replacing the partial derivatives of weight with those for cost.

Table 6.1: Summary of optimization results for Concept 1

b_{min}	Without cost constraint Weight, lb		Cost, labor-hr	
	Mean	Standard Deviation	Mean	Standard Deviation
1.29	69.9	0.81	66.9	0.08
2.33	95.4	0.86	74.0	0.11
3.10	120.0	0.90	81.0	0.14
3.72	144.3	0.93	88.0	0.17
	With cost constraint			
1.29	85.3	0.88	60.2	0.13
2.33	109.0	0.97	66.6	0.16
3.10	133.1	0.98	72.9	0.20
3.72	157.0	1.01	79.2	0.23

The most notable aspect of the results in Table 6.1 is the influence of b_{min}. By tightening the limit on b_{min} from 1.29 to 3.72, the maximum probability of failure in each component is reduced from 0.1 to 0.0001, which results in a weight increase of 84% and 106% with and without cost constraint, respectively. Also by requiring an optimal design at 90% of the cost, the spar weight increases by 22% for $b_{min} = 1.29$ and 8.8% for 3.72.

Table 6.2: Mean weight and mean cost distributions for Concept 1 at $b_{min} = 1.29$

	Without cost constraint			
	Weight, lb	Cost, labor-hr	Part count	Rivet count
Caps	52.6	19.08	2	—
Web	14.9	0.79	3	—
Stiffeners	2.4	1.12	7	—
Assembly	69.9	45.91	12	466
	With cost constraint			
Caps	68.0	12.40	2	—
Web	14.9	0.79	3	—
Stiffeners	2.4	1.12	7	—
Assembly	85.3	45.91	12	466

The weight and cost breakdown for Concept 1 is shown in Tables 6.2 and 6.3 for the two extreme values of b_{min}. It is evident that the major contributors to the overall weight are the spar caps while assembly is the major contributor to the total manufacturing cost. The influence of cost constraint is that it reduces the taper ratio in the horizontal flanges of the caps thereby reducing their machining cost, which is calculated based on the amount of material removed from the original extrusion as indicated by Equations (3.3) and (3.4). The reduction in taper ratio also causes the caps to become heavier, which in turn increases the total spar weight.

As the value of b_{min} is increased, so does the size of the caps and the web thickness when the results in Table 6.2 are compared with those in Table 6.3.

Table 6.3: Mean weight and mean cost distributions for Concept 1 at $b_{min} = 3.72$

| | Without cost constraint | | | |
	Weight, lb	Cost, labor-hr	Part count	Rivet count
Caps	124.5	40.30	2	—
Web	17.0	0.79	3	—
Stiffeners	2.8	1.12	7	—
Assembly	144.3	45.83	12	465
	With cost constraint			
Caps	137.6	31.46	2	—
Web	17.0	0.79	3	—
Stiffeners	2.4	1.12	7	—
Assembly	157.0	45.83	12	465

When $b_{min} = 1.29$, the manufacturing cost of the caps is approximately 29% of the total cost whereas when b_{min} is increased to 3.72 that cost increases to nearly 46%. The change in b_{min} has no impact on manufacturing cost of the web and stiffeners. The assembly cost is also not impacted by the change in b_{min} as the number of fasteners is essentially constant. Based on the cost figures in Tables 6.2 and 6.3, the ratios of recurring to nonrecurring cost for the caps, web, stiffeners, and assembly are found to be 10.2, 5.6, 13, and 12.5, respectively.

The active constraint set at the optimal design point is the same for all b_{min} values with the list shown in Table 6.4. Of the total of 15 design constraints, seven are active. In addition to cost, the list also includes 3 out of four reliability and 3 out of nine manufacturability constraints. The physical-bound constraints address the assembly requirements by allowing adequate space for fastener placement. It appears that the tip displacement constraint has been satisfied indirectly by the large spar caps needed in order to satisfy the reliability constraint in the upper-cap.

Table 6.4: List of active design constraints for Concepts 1 and 2

Type	Constraint Definition	Concept 1	Concept 2
g^c	Total manufacturing cost	A	A
g_1^f	Upper cap reliability index	A	A
g_2^f	Lower cap reliability index		A[a]
g_3^f	Web reliability index	A	A
g_4^f	Stiffener reliability index	A	
g_1^m	Cap section balance	A	A
g_2^m	Cap shape factor		
g_3^m	Cap form factor		
g_4^m	Stiffener section balance		
g_5^m	Stiffener shape factor	A	A
g_6^m	Stiffener form factor		
g_7^m	Physical lower bound on cap ver. flange width	A	A
g_8^m	Physical lower bound on cap hor. flange width		
g_9^m	Physical lower bound on stiffener flange width		A
g^d	Max.tip displacement		

[a] only at $b_{min} = 3.72$ and not the others

Table 6.5 lists the optimal values of design variables for Concept 1 at two values

of b_{min} with and without a cost constraint. The design variable most influenced by

the cost constraint appears to be Y_8, the taper ratio.

Table 6.5: Optimal values of design variables in Concept 1

Design Variable	Random Variable	Without cost constraint	
		$b_{min} = 1.29$	$b_{min} = 3.72$
Y_1	W_1, in.	6.00[a]	6.00[a]
Y_2	t_1, in.	0.32	0.63
Y_3	W_2, in.	2.03	2.31
Y_4	t_2, in.	0.139	0.378
Y_5	W_3, in.	1.95	1.95
Y_6	t_3, in.	0.099	0.121
Y_7	t_{web}, in.	0.091	0.105
Y_8	TR	0.30[b]	0.30[b]
		With cost constraint	
Y_1	W_1, in.	5.80	6.00[a]
Y_2	t_1, in.	0.315	0.62
Y_3	W_2, in.	2.02	2.30
Y_4	t_2, in.	0.147	0.371
Y_5	W_3, in.	1.96	2.08
Y_6	t_3, in.	0.098	0.098
Y_7	t_{web}, in.	0.091	0.105
Y_8	TR	0.62	0.46

[a] Upper bound; [b] Lower bound

6.2 Spar Design Concept 2

The results for Concept 2 are shown in Table 6.6. Similar to Concept 1, the minimum number of intermediate stiffeners needed to achieve a feasible design is seven (see Figure 6.1). With the minimum feasible number of stiffeners, the design is optimized with and without the cost constraint for four different values of b_{min}.

As expected, the use of buckling-type web design in Concept 2 allows the spar weight to decrease by an average of 14.3% over the range of b_{min} considered. Although there is no significant difference between the costs of the two concepts at $b_{min} = 1.29$, Concept 2 becomes cheaper with an increase in b_{min} such that at $b_{min} = 3.72$, it is 8.6% cheaper to build than Concept 1 if the number of parts and fasteners

are kept the same. This cost reduction is made possible only through reduced machining cost of the spar caps.

Table 6.6: Summary of optimization results for Concept 2

b_{min}	Weight, lb		Cost, labor-hr	
	Mean	Standard Deviation	Mean	Standard Deviation
Without cost constraint				
1.29	62.4	0.55	67.0	0.09
2.33	80.4	0.60	72.0	0.11
3.10	95.8	0.63	76.3	0.12
3.72	109.8	0.66	80.3	0.14
With cost constraint				
1.29	72.5	0.61	60.3	0.13
2.33	90.2	0.64	64.8	0.15
3.10	106.2	0.67	68.7	0.18
3.72	121.0	0.68	72.4	0.20

Figure 6.2 shows the plot of optimal weight and the corresponding cost versus b_{min} for the case without the cost constraint. The plot shows that weight escalates at a much faster rate than the cost as b_{min} is increased.

The weight and cost distributions for Concept 2 are shown in Table 6.7. The active constraint set at the optimal design point for $b_{min} = 3.72$ is given in Table 6.3 above. Of the total of fifteen design constraints, 8 are active. In addition to cost, the list also includes 3 out of four reliability constraints and 4 out of nine manufacturability constraints.
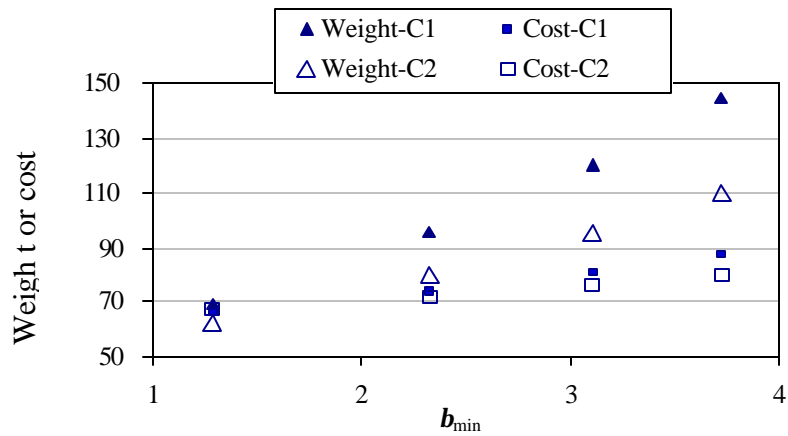
Figure 6.2: Weight and cost variation with reliability for Concept1 (C1) and Concept 2 (C2)

Table 6.7: Mean weight and mean cost distributions for Concept 2 at b_{min} = 3.72

| | Without cost constraint | | | |
	Weight, lb	Cost, labor-hr	Part count	Rivet count
Caps	98.4	32.60	2	—
Web	10.7	0.79	3	—
Stiffeners	0.72	1.12	7	—
Assembly	109.8	45.83	12	465
	With cost constraint			
Caps	110.2	24.66	2	—
Web	10.1	0.79	3	—
Stiffeners	0.71	1.12	7	—
Assembly	121.0	45.83	12	465

Table 6.8 shows the optimal values of design variables for Concept 2 at two values of b_{min} with and without a cost constraint. The design variable most influenced by the cost constraint appears to be Y_8, the taper ratio. However, by increasing the b_{min} value, Y_1 and Y_4 are also influenced by the addition of cost constraint. The most

obvious difference between Concepts 1 and 2 appears to be in the web thickness, Y_7,

stiffener width, Y_5 as well as the vertical flange thickness of the caps, Y_4.

Table 6.8: Optimal values of design variables in Concept 2

Design Variable	Random Variable	Without cost constraint b_{min} 1.29	b_{min} 3.72
Y_1	W_1, in.	4.20	6.00[a]
Y_2	t_1, in.	0.34	0.53
Y_3	W_2, in.	2.05	2.21
Y_4	t_2, in.	0.23	0.29
Y_5	W_3, in.	0.60	0.61
Y_6	t_3, in.	0.104	0.105
Y_7	t_{web}, in.	0.052	0.065
Y_8	TR	0.30[b]	0.30[b]
		With cost constraint	
Y_1	W_1, in.	4.20	4.20
Y_2	t_1, in.	0.33	0.55
Y_3	W_2, in.	2.05	2.26
Y_4	t_2, in.	0.23	0.43
Y_5	W_3, in.	0.60	0.60
Y_6	t_3, in.	0.104	0.104
Y_7	t_{web}, in.	0.053	0.062
Y_8	TR	0.59	0.48

[a] Upper bound, [b] Lower bound

Since the vertical stiffeners help define the aspect ratio of each web panel , thereby influencing the buckling strength, we examined the impact the stiffener spacing reduction could have on the optimal design. For a shear panel, aspect ratio is defined as the ratio of the long side over the short side. Theoretically, the shear-buckling coefficient increases considerably as the panel aspect ratio approaches one. The increase in buckling coefficient allows the panel to become thinner, which could help reduce the total weight of the spar. The results in Table 6.9 are for different values of

NS, which represents the number of evenly spaced intermediate stiffeners in web

Segments 1, 2, and 3 (see Figure 4.1). For all the cases in Table 6.9, $\boldsymbol{b}_{\min}$ is kept at

3.72 and the design is optimized without the cost constraint.

Table 6.9: Effect of *NS* on optimal spar design

NS in segments			Concept 1 Weight, lb	Cost, labor-hr	Concept 2 Weight, lb	Cost, labor-hr
1	2	3				
2	1	0	144.3	88.0	109.8	80.3
3	2	1	144.9	90.9	106.0	83.2
4	3	2	145.4	93.9	106.2	86.1
5	4	3	146.3	96.9	106.5	89.1
6	5	4	146.5	99.9	107.0	92.2

As expected, for both Concepts 1 and 2 the web thickness decreases as *NS* is

increased. However, in Concept 1, the increase in *NS* leads to a growth in the total

spar weight. This apparent contradiction is due to the fact that the weight gained

through addition of more stiffeners is slightly greater than the weight saved through

reduction in web thickness. By contrast, in Concept 2, increasing *NS* leads to a rapid

reduction in total weight followed by a gradual increase beyond what appears to be

the optimal topology for web stiffeners (among the combinations examined) at *NS* =

3, 2, 1 for Segments 1, 2, and 3, respectively. Whereas in Concept 1 the minimum

weight design corresponds to the lowest cost design, in Concept 2 they do not. The

weight reduction of 3.8 lb (3.5%) in going from *NS* = 2,1,0 to *NS* = 3,2,1 in Concept 2

is accompanied by a cost increase of 2.9 labor hours (3.6%).

The effect of *NS* in Concept 2 is explored further with the help of Table 6.10.

The shear stress ratio in the last column gives an indication of the load carried by the

web panel near the spar root. Although the largest k occurs in the case $NS = 4,3,2$, the lightest design corresponds to $NS = 3,2,1$.

Table 6.10 Effect of NS in Concept 2

NS in segments 1 2 3			k	$Y_7, t_{web,}$,$in.$	t / t_{cr}
2	1	0	0.080	0.0650	1.44
3	2	1	0.357	0.0420	5.58
4	3	2	0.358	0.0399	5.62
5	4	3	0.353	0.0392	5.47
6	5	4	0.332	0.0396	4.91

A closer examination of the results indicated that the size of web stiffeners has reached the minimum value imposed by the manufacturability constraint and cannot become any smaller as their quantity increases. There is also very minor change in the cap dimensions as a result of changing NS. So the fact that $NS = 3,2,1$ gives the lightest weight is due to the combination of cap size and web thickness.

6.3 Design Sensitivity Analysis

Equation (2.11-a) is used to calculate the probabilistic sensitivity derivatives of each safety index with respect to the mean value of individual random variables identified in Table 4.2. These sensitivities are calculated at the optimal design point and normalized as

$$\left. \frac{\partial b}{\partial m_{X_i}} \right|_{x^*}^n = \left. \frac{\partial b}{\partial m_{X_i}} \right|_{x^*} \left(\frac{m_{X_i}}{b} \right) \qquad (6.2\text{-a})$$

$$\left.\frac{\partial b}{\partial s_{X_i}}\right|_{x^*}^{n} = \left.\frac{\partial b}{\partial s_{X_i}}\right|_{x^*}\left(\frac{s_{X_i}}{b}\right) \qquad (6.2\text{-}b)$$

The plots of normalized sensitivities obtained from Equation (6.2-a) for Concept 1 are shown in Figure 6.3.
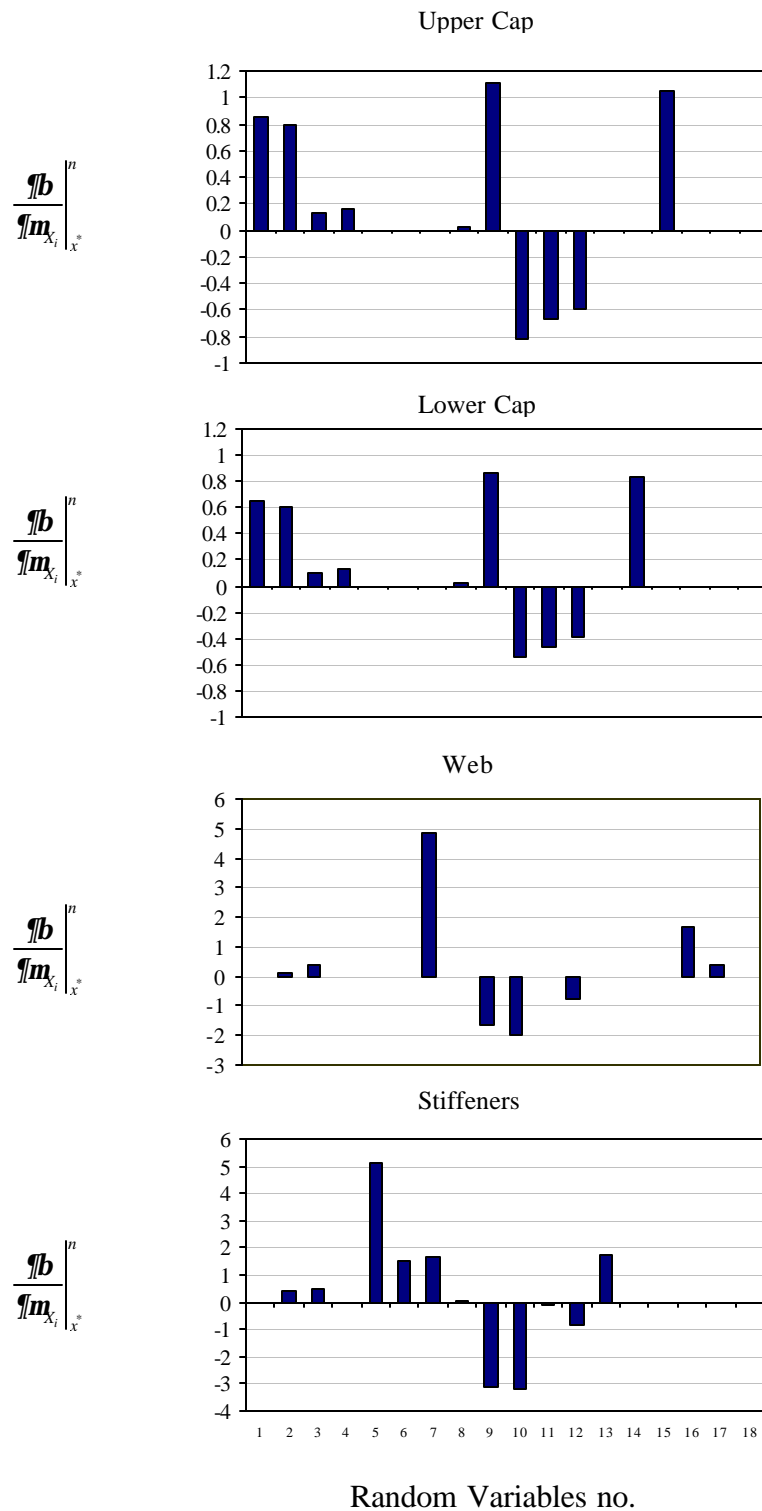
Figure 6.3: Plot of reliability sensitivity derivatives for Concept 1 obtained from Equation. (6.2-a)

As indicated in Figure 6.3, the reliability of the upper cap is influenced most by the spar height at the root, H_1 followed closely by the compressive yield strength of the cap material.

In applying the Gerard method for calculation of the crippling stress for a Tee section, an upper limit of 80% compressive yield stress is used [67]. Hence, if the calculated crippling stress is less than the limit, then the Gerard formula, which is a function of Young's modulus, is used. Otherwise, the crippling stress is set equal to the upper limit. For the optimal design in Concept 1, the calculated crippling stress in the upper cap has exceeded the 80% limit and that explains the lack of sensitivity to the Young' modulus. The reliability sensitivities for the lower cap show the spar height at the root and the tensile yield strength of the material as having the most influence on b_{min}.

For the web, the most influential random variable is the web thickness followed by the spar length while for the web stiffeners, the stiffener flange width has the most influence on stiffener's reliability followed by spar length and height.
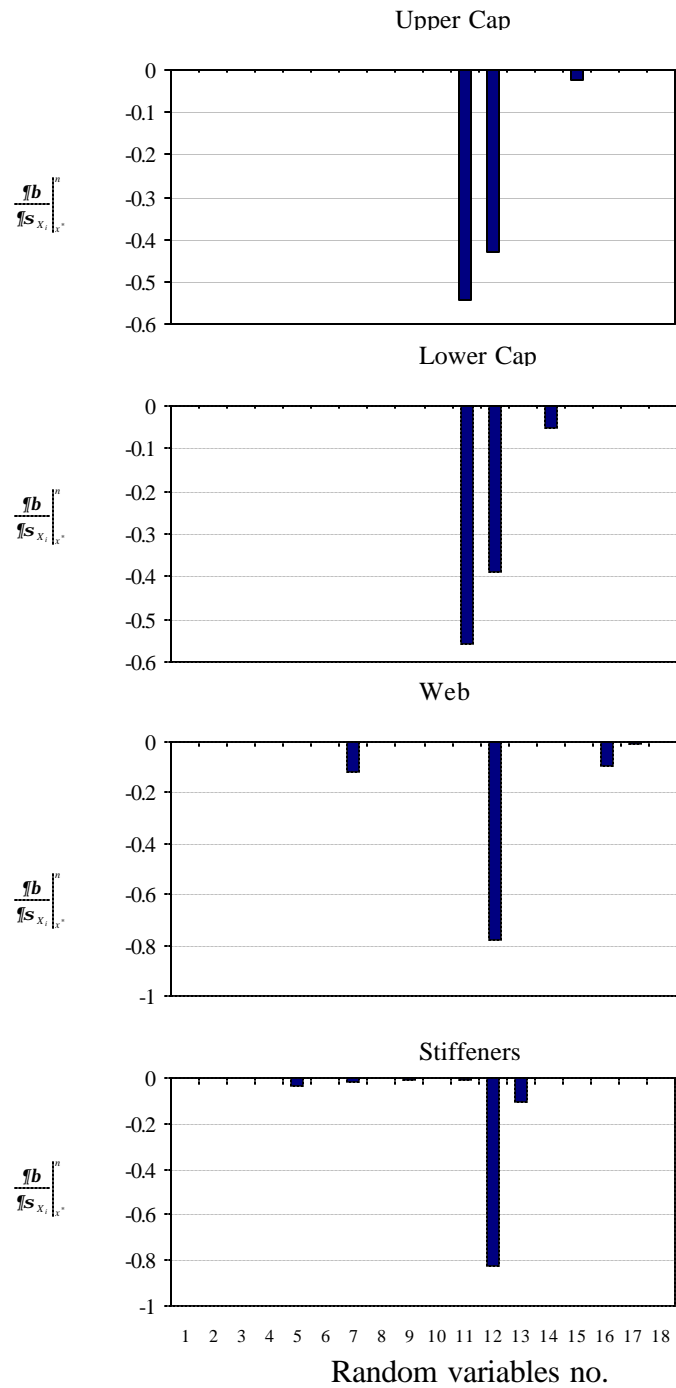
Figure 6.4: Plot of reliability sensitivity derivatives for Concept 1 obtained from Equation (6.2-b)

The plot of sensitivities obtained from Equation (6.2-b) is presented in Figure 6.4. These sensitivities indicate the effect of scatter in each random variable on the reliability of individual structural members in Concept 1. As indicated, b_{min} in all structural parts is most sensitive to the scatter in random variables 11 and 12 describing the loading parameters, *d* and *p* (see Table 4.2).

The plots of reliability sensitivities for Concept 2 are shown in Figure 6.5. The reliability of the upper cap appears to be most sensitive to the values of horizontal flange thickness and the spar height at the root followed by the compressive yield strength of the material. The effects of spar length and load parameters are also evident in the plot.

The lower cap is slightly more sensitive to the spar height at the root and the tensile yield strength of the material than the horizontal flange dimensions. The influences of spar length and the load parameters are strong in this case also but less so than for the upper cap. The influence of length is most pronounced on reliability of the web and web stiffeners followed by the web thickness. The sensitivity plots obtained from Equation (6.2-b) for Concept 2 are fairly similar to those for Concept 1, hence, are not included here.

With the influence of random variables 9 through 12 (see Table 4.2) more widespread than others, we tested Concept 1 by changing the distribution type of these four random variables from Normal to Lognormal. The results of optimization without a cost constraint at $b_{min} = 3.72$ are shown in Table 6.11.
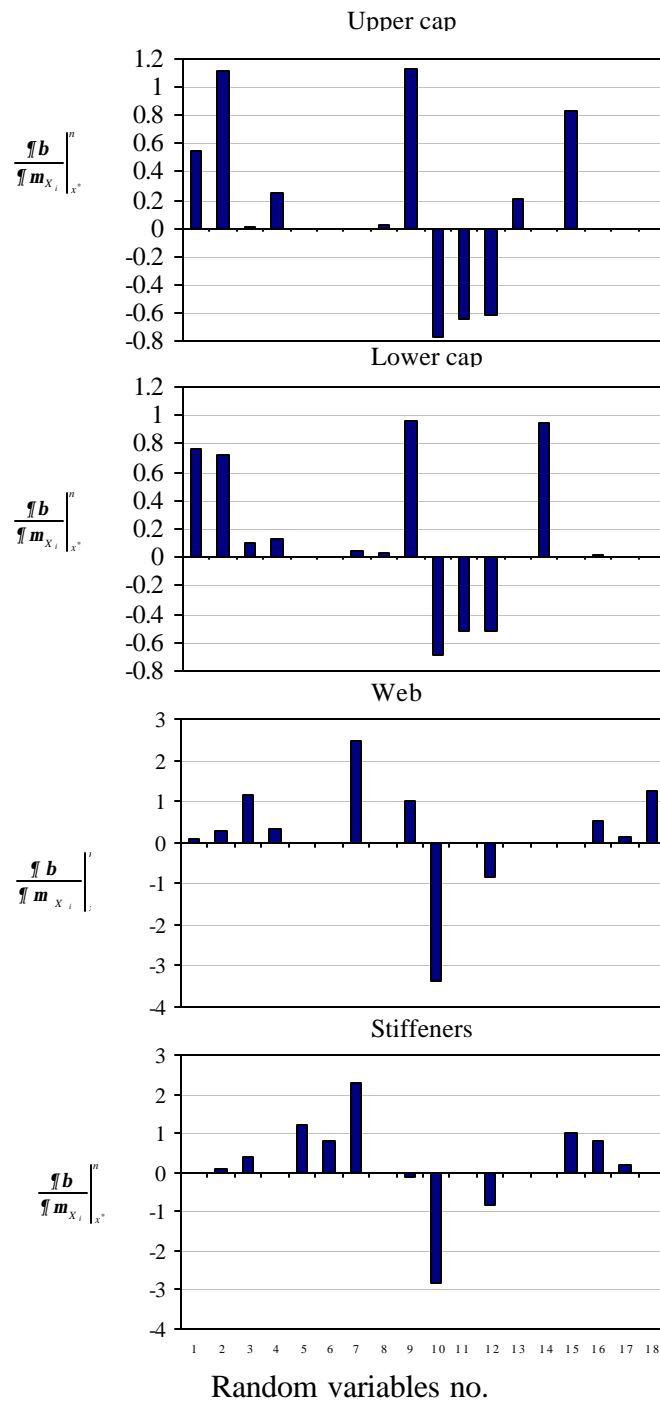
Figure 6.5: Plot of reliability sensitivity derivatives for Concept 2 obtained from Equation (6.2-a)

Table 6.11: Optimal values of design variables in Concept 1 with random variables 9-12 having lognormal distribution

Design Variable	Random Variable	$b_{min} = 3.72$
Y_1	W_1, in.	6.00[a]
Y_2	t_1, in.	0.87
Y_3	W_2, in.	2.54
Y_4	t_2, in.	0.60
Y_5	W_3, in.	1.95
Y_6	t_3, in.	0.129
Y_7	t_{web}, in.	0.114
Y_8	TR	0.30[b]

[a] Upper bound, [b] Lower bound

The optimal mean weight is 214.6 lb at a mean cost of 101.5 labor hours. The mean weights of caps, webs, and stiffeners are 193.4, 18.4, and 2.9 lb, respectively, and the mean costs for the caps, web, stiffeners, and assembly are found to be 54.0, 0.79, 1.12, and 45.67 labor hours, respectively.

CHAPTER VII

SYSTEM RELIABILITY ANLYSIS AND OPTIMIZATION

Up to this point, we treated the four component reliability indices independently and placed a constraint on each of them as demonstrated in Concepts 1 and 2. However, since the system probability of failure may be lower than that for the most critical component [45], we must perform a system reliability analysis and repeat the design optimization based on system reliability requirement. In this chapter, we will discuss system reliability analysis and present the results for system reliability-based optimization (SRBO) for the wing spar in Concept 1.

7.1 System Reliability Analysis

Practical engineering structures usually consist of many interconnected components whose failures may not necessary lead to the failure of the whole system. Consequently, the reliability of the most critical member may not be representative of the reliability of the whole system. Hence, it is necessary to evaluate structural reliability at the system level in order to obtain a more meaningful insight into the whole system.

According to Nowak [50] it is possible to model a system as a series system if the entire system failure is triggered by failure of a single member, and as a parallel

system if the system does not fail unless all members fail simultaneously. It is also possible to model a system as a combination of series and parallel systems.

If there is no correlation between any two elements in a series system, the probability of system failure can be evaluated as

$$P_f = 1 - \prod_{i=1}^{n} [1 - P_{f_i}] \qquad (7.1)$$

where P_{f_i} is the probability of failure of the *ith* element and n is the number of elements. For a parallel system with no correlation among its elements, the probability of system failure can be obtained as

$$P_f = \prod_{i=1}^{n} P_{f_i} \qquad (7.2)$$

For a hybrid system, the probability of system failure can be determined by first calculating the probabilities of failure of parallel subsystems, which can subsequently be represented by an equivalent component. By simplifying the total system to an equivalent series system, the probability of system failure can be calculated using the same procedure as for a simple series system. Obviously, under no correlation assumption, the probability of failure for a series system is greater than or equal to that for a single member, whereas for a parallel system, the probability of failure is less than or equal to the smallest element probability of failure.

In Chapter IV, it was assumed that the element failures are uncorrelated. In fact, it is likely for the system elements to be correlated due to common source of materials, similar manufacturing process, common random variables, and common sources of load, etc. The reliability analysis for this type of system is discussed next.

7.1.1 Reliability of a Parallel System

For parallel systems, as stated by Madsen et al. [53], the failure set is approximated by the intersection of the sets outside the tangent hyper-planes at corresponding most probable points of failure.

The probability of failure for a parallel system can be computed as [27]

$$P_f = p(\bigcap_{i=1}^{n} \{g_i(X) \leq 0\}) \approx \Phi_n(-\beta; \rho)$$

(7.3)

where $g_i(X)$ is the *ith* limit state function for the system, $\boldsymbol{b}$ is the component reliability index vector, $\Phi_n(-\boldsymbol{b}; \boldsymbol{r})$ is the standard multinormal integral with correlation coefficients matrix $\boldsymbol{r} = [\boldsymbol{r}_{ij}]$ with

$$\boldsymbol{r}_{ij} = \sum_{k=1}^{n} \boldsymbol{a}_{ik}\boldsymbol{a}_{jk}$$

(7.4)

where $\boldsymbol{a}_{ik}$ and $\boldsymbol{a}_{jk}$ are the *kth* direction cosines at the most probable point for the *ith* and *jth* limit state functions, respectively, and *n* is the number of independent random variables.

7.1.2 Reliability of a Series System

For a series system, the failure set is approximated by the polyhedral set bounded by the tangent hyper-planes at most probable points with the probability of failure computed as [27]

$$P_f = P(\bigcup_{i=1}^{n} \{g_i(X) \leq 0\}) \approx 1 - \Phi_n(\boldsymbol{b}; \boldsymbol{r})$$

(7.5)

where $\boldsymbol{b}$ and $\boldsymbol{r}$ have the same definition as in Equation (7.3).

A very narrow bound suggested by Ditlevsen [53] is widely used to estimate the probability of failure for series systems. The bound is expressed as

$$P_1 + \sum_{i=2}^{k} \max\left\{ P_i - \sum_{j=1}^{i-1} P_{ij}, 0 \right\} \leq P_F \leq \sum_{i=1}^{k} P_i - \sum_{i=2}^{k} \max_{j<i} P_{ij} \tag{7.6}$$

where $P_i = P(g_i(X) \leq 0)_i \approx \Phi(-\mathbf{b}_i)$ and $P_{ij} = P(g_i(X) \leq 0 \cap g_j(X) \leq 0)$, which can be computed as

$$P_{ij} \approx \Phi(-\mathbf{b}_i, -\mathbf{b}_j; \mathbf{r}_{ij}) = \int_{-\infty}^{-\mathbf{b}_i} \int_{-\infty}^{-\mathbf{b}_j} \mathbf{j}(x, y; \mathbf{r}_{ij}) dx dy \tag{7.7}$$

where $\mathbf{j}(x, y; \mathbf{r})$ is the probability density function for bivariate normal vector with zero mean value, unit variance, and correlation coefficient $\mathbf{r}$, and is expressed as

$$\mathbf{j}(x, y; \mathbf{r}) = \frac{1}{2\mathbf{p}\sqrt{1-\mathbf{r}^2}} \exp\left[-\frac{1}{2} \frac{x^2 + y^2 - 2\mathbf{r}xy}{1-\mathbf{r}^2} \right] \tag{7.8}$$

The bounds depend on the numbering of failure modes. Ranking the failures modes according to decreasing probability of failure is considered to be a good scheme.

7.1.3 Reliability of Series System of Parallel Subsystems

A complex structural system can be modeled as a series system of parallel subsystems with its probability of failure computed as

$$P_f = P\left[\bigcup_{i=1}^{K}(\bigcap_{r=1}^{l_i}(\{g_{ir} \leq 0\}))\right]$$

(7.9)

Where k is the number of subsystems and l_i is the number of elements in the *ith*

parallel subsystem [53].

7.2 System Reliability Evaluation for Wing Spar

For system reliability analysis, the wing is divided into separate cap, web, and stiffener elements as shown in Figure 7.1. The stiffener at the root is excluded, as it normally would be designed based on other design criteria. We assume that the system will fail if any one of the following events occurs:

- Failure in any one of upper cap elements

- Failure in any one of lower cap elements

- Failure in any one of panel webs

- Failure in any one of stiffeners
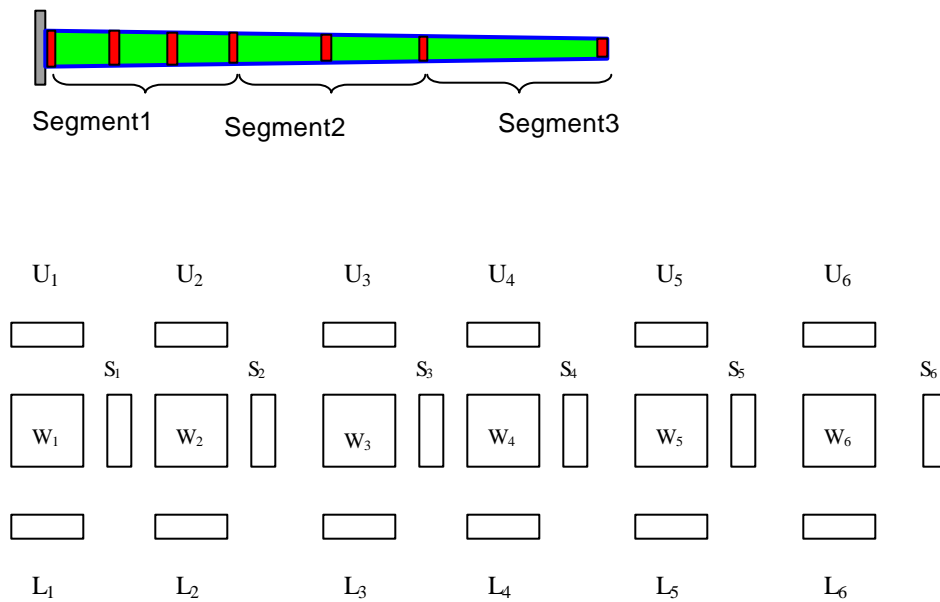
Figure 7.1: Wing spar model for SRBO

Because the wing spar is treated as a statically determinate structure, its fault tree model is constructed using "or" gates as shown in Figure 7.2 with the top event defining system failure as a result of any of the failure events shown below it. The spar is modeled as a series system consisting of four separate subsystems, i.e., upper cap, lower cap, web, and stiffener subsystems with each having six serially connected elements.
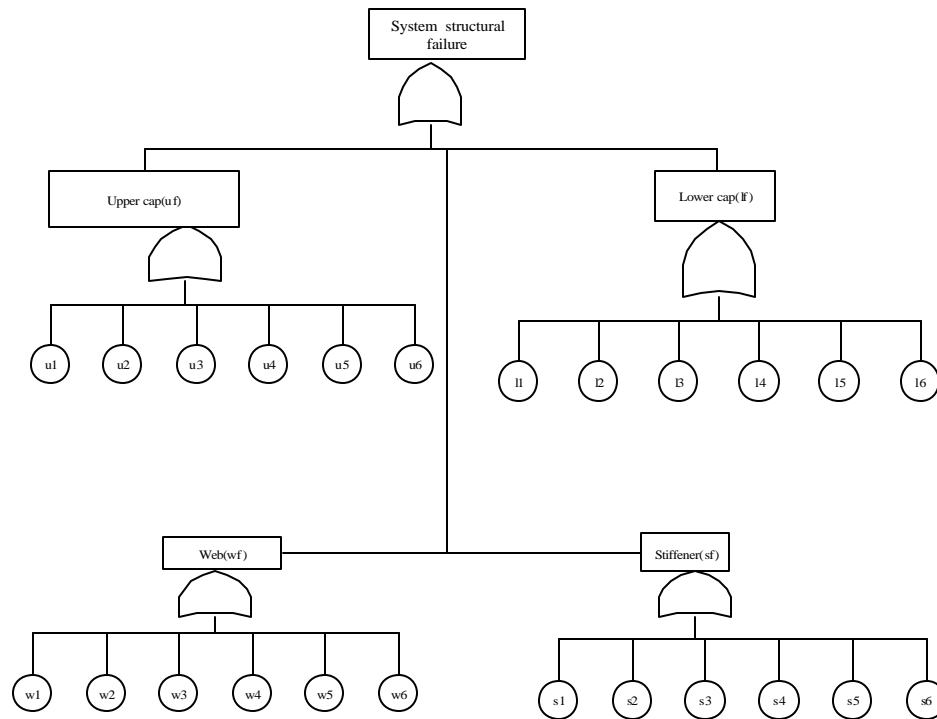
Figure 7.2 Fault tree model of wing spar

The probability of system failure is expressed mathematically as

$$P_f = P[uf \cup lf \cup wf \cup sf] \tag{7.10}$$

where *uf, lf, wf, and lf* are the failure events for the upper cap, lower cap, web, and stiffeners with each subsystem probability of failure computed as

$$P(uf) = P[(u1 \cup u2 \cup u3 \cup u4 \cup u5 \cup u6)] \tag{7.11}$$

$$P(lf) = P[(l1 \cup l2 \cup l3 \cup l4 \cup l5 \cup l6)] \tag{7.12}$$

$$P(wf) = P[(w1 \cup w2 \cup w3 \cup w4 \cup w5 \cup w6)] \tag{7.13}$$

$$P(sf) = P[(s1 \cup s2 \cup s3 \cup s4 \cup s5 \cup s6)] \tag{7.14}$$

In Equations (7.11-7.14), u_i, l_i, w_i are the failure events of the *ith* element of upper cap, lower cap, and the web, respectively whereas s_i is the failure event of the *ith* stiffener.

To obtain the system probability of failure of the wing spar, the main procedure includes: (i) calculating the reliability indices of individual elements using DOT; (ii) converting the original system into a system with three equivalent components; (iii) computing the system reliability using Ditlevsen's upper bound theory. Figure 7.3 illustrates the flow chart for the evaluation of system reliability index.
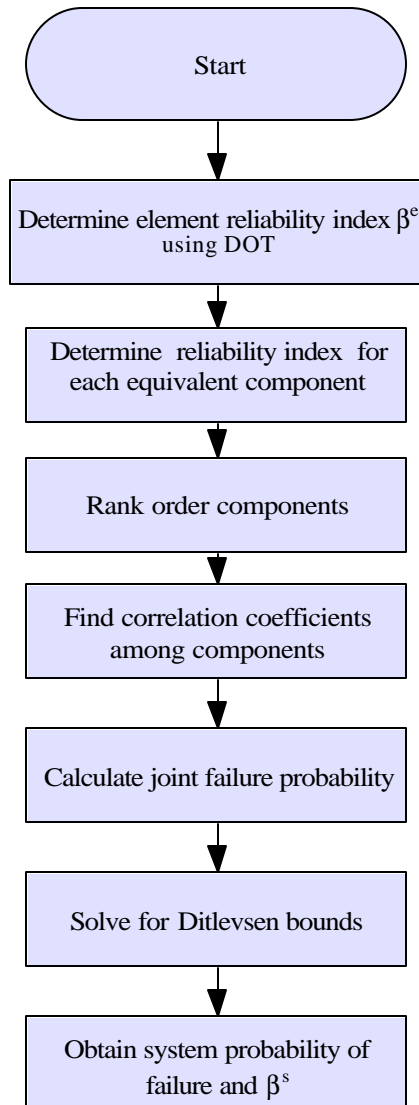
Figure 7.3: Flow chart for the evaluation of system reliability index

To obtain the reliability indices of individual elements, $\boldsymbol{b}^e$, a robust SQP [54] rather than HL-RF algorithm is used to avoid convergence problems.

Two steps are used to convert the original system into a system with three equivalent components. The first step is to reduce each subsystem to an equivalent component. Taking the upper cap subsystem as an example, there are six constituent elements in series as shown in Figure 7.4, which can be converted to an equivalent component *Ue.*
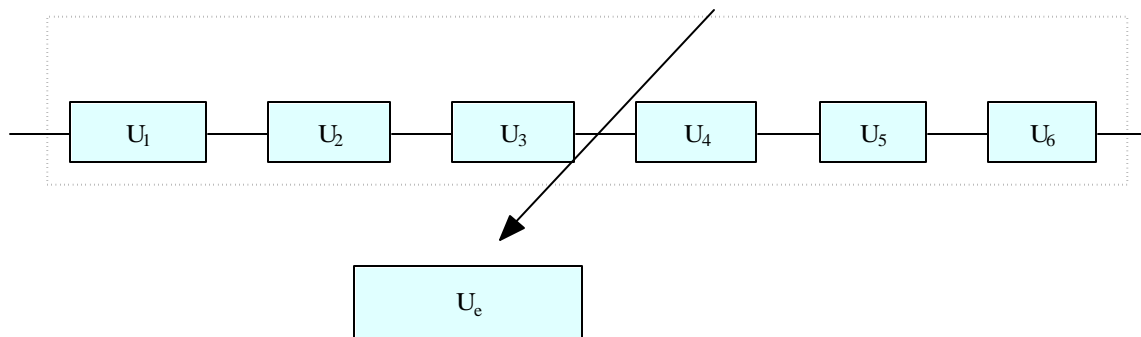
Figure 7.4:Reduction of the upper cap series subsystem

The probability of failure of the upper cap subsystem can be computed using Equation (7.4) with correlations between different failure modes evaluated using direction cosines. If all the elements in the upper cap subsystem are fully correlated ($\boldsymbol{r}_{ij}$=1), the probability of failure will correspond to the largest probability of failure among the constituent elements [50]. Likewise, The lower cap, web, and stiffener subsystems can be simplified into equivalent components that are depicted as L_e, W_e, S_e repectively in Figure 7.5. The wing spar system is thus reduced to a series system with four components as shown in Figure 7.5.
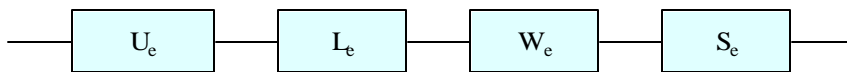
Figure 7.5: Reduced wing spar system with four equivalent components

The second step is to further reducing the system to one consisting of only three equivalent components by replacing U_e and L_e with an equivalent component UL_e, see Figure 7.6.
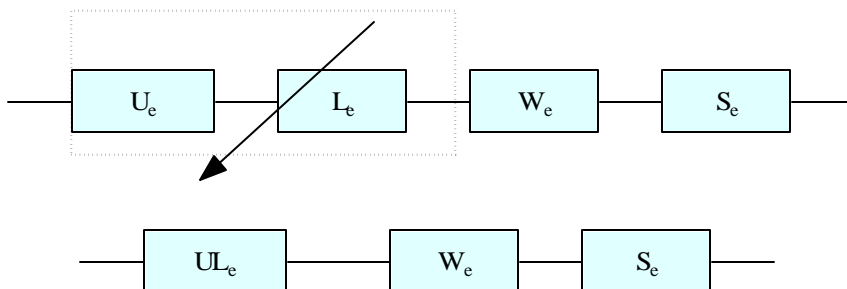
Figure 7.6: Reduction of wing spar system to three equivalent components

Then Ditlevsen's upper bound theory is employed to compute the probability of failure of the system that is shown in Figure 7.7.
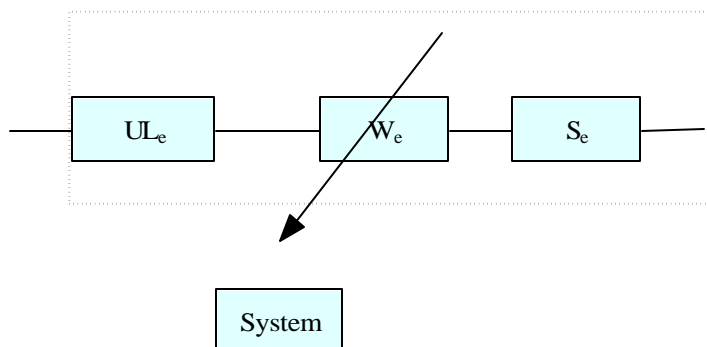
Figure 7.7: Equivalent single component of wing spar system

The presented method was used to evaluate the system reliability index associated with the optimum design for Concept 1 in Chapter VI.

The correlation coefficients among different failure modes are needed to obtain the equivalent components and the system probability of failure. Equation 7.15 shows the correlation coefficient matrix for upper cap obtained using the Equation 7.4.

$$
\begin{bmatrix}
1 & & & & & \\
.999 & 1 & & & & \\
.996 & .999 & 1 & & & \\
.988 & .994 & .998 & 1 & & \\
.974 & .983 & .991 & .997 & 1 & \\
.951 & .963 & .976 & .987 & .996 & 1
\end{bmatrix}
\tag{7.15}
$$

where r_{ij} is the correlation coefficient between the failure modes of the ith and jth elements of upper cap. It is evident that failure modes in the upper cap elements are almost fully correlated. Therefore, the equivalent component for the upper cap subsystem is the one with the largest probability of failure, i.e., U_1. Likewise, L_1, $W1$, and S_1 are the equivalent components for the lower cap, web, and stiffener subsystems respectively. Hence, the wing spar system is simplified to a series system as shown in Figure 7.8. Using Equation 7.4, the correlation coefficient between U_1 and L_1 is found to be 0.961, which is close to 1. U_1 can thus be approximately treated as the equivalent component for U_1 and L_1. The system is then simplified to a series with only three components as shown in Figure 7.9 for which the system probability of failure can be evaluated using Ditlevsen's upper bound theory.

The computed system reliability is found to be 3.47, which is 6.7% smaller than the smallest component reliability index, 3.72. This means the component reliability-

based optimization cannot guarantee the safety of the system. Therefore, system reliability-based optimization is needed to assure a safe design.
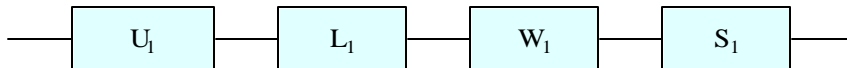
Figure 7.8: Simplified system with four components
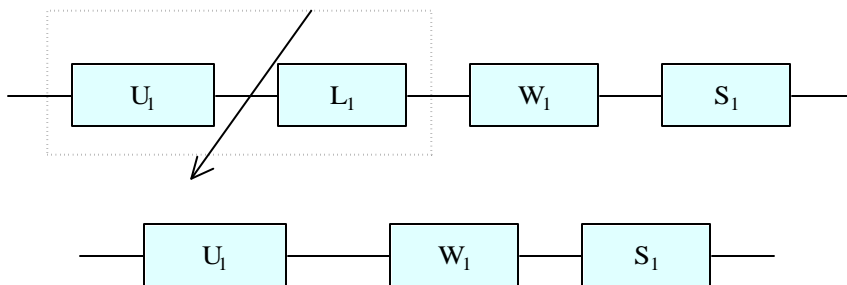
Figure 7.9: Simplified system with three components

7.3 System Reliability-Based Optimization

System reliability-based optimization (SRBO) is formulated as

$$\text{Minimize} \qquad f(\boldsymbol{X})$$

Subject to:

$$
\begin{aligned}
&g^{d}(X) \leq 0 \\
&g_{i}^{m}(X) \leq 0, \qquad i=1,2,...,NM \\
&g^{c}(X) \leq 0 \\
&g^{s_f}(X) \leq 0
\end{aligned}
\tag{7.16}
$$

$$Y_k^l \leq Y_k \leq Y_k^{u}, \qquad k=1,2,...,NDV$$

where g^{s_f} represents the constraint on system reliability index, which is expressed as

$$1 - \frac{\boldsymbol{b}^{s}}{\boldsymbol{b}^{s_{\min}}} \leq 0 \tag{7.17}$$

where $\boldsymbol{b}^{s}$ is the system reliability index of the wing spar and $\boldsymbol{b}^{s_{\min}}$ is the target system reliability index. Other terms in Equation (7.16) have the same definition as in Equation (4.4).

In this thesis, system reliability-based optimization without cost constraint has been performed only for Concept1. A two–level strategy suggested by Enevoldsen and Sorensen [40] was employed to do the system reliability-based optimization. At the top level, DOT was used to solve the optimization problem formulated in Equation (7.16). Also DOT was utilized to estimate components reliability indices for the evaluation of the system reliability index. Optimization results for Concept 1 have been summarized in Table 7.1.

Table 7.1 Summary of SRBO results for Concept1

β_{min}	Weight, lb		Cost, labor-hr		CPU time, s	
	1	2	1	2	1	2
1.29	69.9	77.7	66.9	68.2	42	920
2.33	95.4	104.3	74.0	75.3	38	479
3.10	120.0	127.6	81.0	82.5	29	1089
3.72	144.3	149.9	88.0	88.4	30	914

1:Results of component reliability-based optimization
2:Results of system reliability-based optimization

From Table 7.1, we find that the system reliability-based optimization resulted in a heavier weight and a higher cost than that of the component reliability-based optimization for all target reliability indices examined. The weight increase from component reliability-based to system reliability-based optimization is approximately 11.1%, 9.3%, 6.3%, and 3. 9%, for target reliability index of 1.29, 2.33, 3.10, and 3.72, respectively. The cost increase is comparatively small, which is approximately 0.45%, 1.85%, 1.76% and 1.94%.

Computational time for system reliability-based optimization presented in Table 7.1 is recorded by running the system reliability-based optimization code on a SUNW, Ultra-Enterprise server (SunOS 5.8). For $b^{s_{min}} =3.72$, the computational time is over thirty times that for component reliability-based optimization.

CHAPTER VIII

SUMMARY AND CONCLUSIONS

In this thesis, we discussed the probabilistic design optimization of aircraft structures based on requirements associated with safety, producibility, and affordability in presence of parametric uncertainty. The design methodology presented was developed into a computer program and applied to a built-up wing spar design problem with two alternative web design concepts (i.e., non-buckling and buckling).

Of all constraints, the cost and component reliability proved to be most dominant. The main influence of the cost constraint was to increase the cap taper ratio thereby reducing its machining cost. Among the manufacturability constraints, section balance had the most influence on the cap design followed by the physical-bound constraint for the stiffener.

The use of buckling-type web design in Concept 2 reduced the overall weight of the spar as the web was allowed to carry load beyond buckling in the form of diagonal semi-tension field action. Although the weight in Concept 2 was 14% less than Concept 1, there was no appreciable difference in the manufacturing cost, which is dominated by the assembly cost.

The tightening of target reliability index from 1.29 to 3.72 caused the weight to increase by an average of 90% for Concept 1 and 70% for Concept 2 and increased the cost by more than 30% and 20%, respectively, both primarily as a result of growth in spar cap dimensions. The assembly cost stayed constant because of the number of fasteners. A closer examination revealed that the 2-in. upper bound on fastener spacing was the reason.

The reduction in stiffener spacing (i.e., increasing the number of stiffeners) resulted in an overall weight increase for Concept 1. However, for Concept 2, the use of 10 stiffeners led to the lowest-weight spar design.

The most influential random variables affecting component reliability were identified. The changing of the distribution type on spar height at the root, spar length, and loading parameters from normal to lognormal resulted in a 49% increase in weight and 15.4% increase in cost.

The component reliability-based optimization cannot guarantee the safety of the wing spar structural system. The correlation between elements should be taken into account to obtain the system reliability index.

The system reliability-based optimization generated a safer design than that obtained using component reliability-based optimization.

The weight increase from component reliability-based to system reliability-based optimization is at least 3. 9% four prescribed target reliability indices: 1.29, 2.33, 3.10, and 3.72. The cost increase is comparatively small, which is less than 2%.

To extend the research presented in this thesis, the following recommendations are made:

- Expand the manufacturability analysis capabilities to include machining and forming process.

- Extend the system reliability analysis to large aircraft structural systems (e.g., wing) for which finite element analysis may have to be used for evaluation of the limit state functions.

- Include damage tolerance analysis and fracture failure at riveted joints.

REFERENCES

[1] Gupta, S. K., Das, D., Regli, W. C., and Nau, D. S., "Current Trend and Future Challenges in Automated Manufacturability Analysis," Technical Research Report No. 95-16, Institute for Systems Research, University of Maryland, 1995.

[2] Boothroyd, G., Dewhurst, P, and Knight, W., Product Design for Manufacture and Assembly, Marcel Dekker, Inc., New York, 1994.

[3] Kessler, W. C., Shumaker, G. C., and Hitchcock, M. F., "Early manufacturing considerations in design, "Paper No. N94-24315, presented at an AGARD Meeting on Integrated Airframe Design Technology, April 1993.

[4] El-Gizawy, A. S., Hwang, J.Y., and Brewer, D. H., "A strategy for integrating product and process design of aerospace components," *Manufacturing Review*, vol. 3, No. 3, September 1990, pp. 178-186.

[5] Boothroyd, G. and Radovanovic, P., "Estimating the cost of machined components during the conceptual design of a product", Anals of the CIRP, vol.38, 1989,pp157-160.

[6] Hu,W., and Polia,C., "To injection mold, to stamp, or to assemble? A DFM cost perspective", Journal of Mechanical Design, vol.121, 1999, pp461-469.

[7] Gupta.,S.K., "Using manufacturing planning to generate manufacturability feedback", Journal of Mechanical design , vol.119, 1997,pp73-80.

[8] Subramaniam, B. L. and Ulrich, K. T., "Producibility analysis using metrics based on physical models," *Design Engineering*, Vol. 68, Design Theory Methodology, ASME 1994, pp. 353-369.

[9] Shankar, S.R. and Jansson, D.G., "A generalized methodology for evaluating manufacturability," Concurrent Engineering, Contemporary Issues and Modern Design Tools, edited by Parsaei, H.R. and Sullivan, W.G., Chapman and Hall Publishers, 1993, pp. 248-263.

[10] Rais-Rohani, M., "A framework for preliminary design of aircraft structures based on process information," Final Report, Parts 1 and 2, NASA Grant NAG-1-1716, December 1998.

[11] Harry, M. J. and Lawson, J. R., Six Sigma Producibility Analysis and Process Characterization, Motorola University Press, 1992.

[12] Ayyub, B. and Mccuen, R.H., Probability, Statistics, & Reliability for Engineers, CRC Press LLC, 1997.

[13] Shinozuka, M., "Basic analysis of structural safety," *Journal of the Structural Division*, ASCE, Vol. 109, No. 3, 1983, pp. 721-740.

[14] Harbitz, A. and Veritas, D.N., "Efficient and accurate probability of failure calculation by use of the importance sampling", Fourth International Conference on Applications of Statistics and Probability in Soil and Structural Engineering, 1983, pp825-836.

[15] Hasofer, A.M. and Lind, N. "An exact and invariant first-order reliability format", *Journal of Engineering Mechanics* Vol. 100, 1974, pp.111-121.

[16] Rackwitz, R. and Fiessler, B., "Structural Reliability under Combined Random Load Sequences," *Computers and Structures*, Vol. 9, No.5, 1978, pp. 489-494.

[17] Hohenbichler, M. and Rackwitz, R., "First-order in system reliability," Structural Safety, v 1, 1983, pp 177-188.

[18] Gollwitzer and Rackwitz,R. ,"Equivalent components in first-order system Reliability", Reliability Engineering, v 5, 1983, pp 99-115.

[19] Enevoldsen,I. and Sorensen,J.D., "Reliability-based optimization of series systems of parallel systems", Journal of Structural Engineering, vol.119,1993, pp1069-1084.

[20] Fissler, B.,Neumann H.-J. and Rackwitz R., "Quadratic limit states in structural relaibility," Journal of the Engineering Mechanics Division,Vol.105,1979, pp661-676.

[21] Breitung, Karl, "Asymptotic approximations for multi-normal integral," Journal of Engineering Mechanics, v 110, 1984, pp 357-366.

[22] Tvedt, L., "Distribution of quadratic forms in normal space—Application to structural reliability," Journal of Engineering Mechanics, vol. 116, 1990, pp. 1183-1197.

[23] Der Kiureghian, A., Lin, H.Z. and Hwang, S.J., "Second-order reliability approximations ", Journal of Engineering Mechanics, v 113,1987, pp 1208-1225.

[24] Der Kiureghian, Armen, De Stefano and Mario, "Efficient algorithm for Second-order reliability analysis", Journal of Engineering Mechanics, v 117, Dec, 1991, pp 2904-2923.

[25] Koyluoglu, Hasan Ugur and Nielsen, Soren R.K., "New approximations for SORM integrals", Structural Safety, v 13, n 4, Apr, 1994, p 235-246.

[26] Zhao, Yan-Gang and Ono, Tetsuro, "New approximations for SORM: Part 1 and 2 ", Journal of Engineering Mechanics, v 125, pp 79-93.

[27] Hohenbichler, M.,Gollwitzer ,S.,Kruse W. and Rackwitz,R., "New light on first and second-order reliability methods," Structural Safety,1987, pp267-284.

[28] Zhao, Y.G. and Ono, T., "System reliability evaluation of ductile frame structure," *Journal of Structural Engineering*, v 124, 1998, pp 678-685.

[29] Bucher, C.G. and Bourgund, U.**, "**Fast and efficient response surface approach for structural reliability problems,**"** Structural *Safety*, v 7, 1990, pp 57-66.

[30] Mahadevan, S., Shi, P., Salter, J. and Raghothamachar, P.**, "**Advanced reliability methods", AIAA/ASME/ASCE/AHS/ASC Structures, Structural Dynamics and Materials Conference, v 4, 1999, pp 3026-3034.

[31] Rais-Rohani, M., and Singh, M. N., "Efficient response surface approach for reliability estimation of composite structures," Proceedings of the 9th AIAA/ISSMO Symposium on Multidisciplinary Analysis and Optimization, Atlanta, GA, September 4-6, 2002.

[32] Shao, S. and Murotsu, Y., "Structural reliability analysis using a neutral network," JAME International Journal, Series A, vol.40, 1997, pp242-246.

[33] Rais-Rohani, M. and Huo, Z., "Analysis and optimization of primary aircraft structures based on strength, manufacturability, and cost requirements," Proceedings of the 40th AIAA/ ASME/ASCE/AHS/ASC Structures, Structural Dynamics and Materials Conference, St. Louis, MO, April 12-15, 1999.

[34] Fenyes, P., "Structural optimization with manufacturing considerations," Proceedings of the 33rd AIAA/ASME/ASCE/AHS/ASC Structures, Structural Dynamics and Materials Conference, Dallas, TX, April 13-15, 1992, pp. 638 - 647.

[35] Martinez, M. P., Messac, A., and Rais-Rohani, M., "Manufacturability-based optimization of aircraft structures using physical programming," *AIAA Journal*, Vol. 39, No. 3, Mar. 2001, pp. 517-542.

[36] Frangopol, Dan M., "Sensitivity of reliability-based Optimum Design ", Journal of Structural Engineering, v 111, 1985, pp 1703-1721.

[37] Fu, G. and Frangopol, D. M., "Reliability-based vector optimization of structural systems" Journal of Structural Engineering, v 116,1990, pp 2143-2161.

[38] Yang,J.S. and Nikolaidis, E., "Design of aircraft wings subjected to gust loads. A safety index based approach" AIAA Journal, 29,191, pp804-812.

[39] Yang, L. and Ma, Z.K., "Optimum design based on reliability for a composite structural system", Computers and Structures, v36, 1990, pp785-790.

[40] Enevoldsen,I. and Sorensen, J.D., "Reliability-based optimization in structural engineering", Structural Safety,v15,1994, pp169-196.

[41] Royset, J.O., Der Kiureghian A., and Polak, E.,"Reliability-based optimal design of series structural systems," Journal of Engineering Mechanics, vol.127, 2001, pp607-614.

[42] Kuschel, N. and Rackwitz,R., "Two basic problems in reliability-based structural optimization", Mathematical Methods of Operation Research ,vol.46, 1997,pp309-333.

[43] Feng, Y. S. and Moses, F., "Methods of structural optimization based on structural system reliability", Journal of Structural Mechanics, v 14, 1986, pp 437-453.

[44] Lee, J.O, Yang, Y.S. and R, W.S., "A comparative study on reliability-index and target-performance-based probabilistic structural design optimization ", Computers and Structures, v 80, 2002, pp 257-269.

[45] Wang, L. and Grandhi, R.V., "System reliability analysis optimization with the use of higher-order approximations, AIAA-96-4043-CP, 1996, pp579-591.

[46] Frangopol, D.M. and Maute, K., "Life-cycle reliability-based optimization of Civil and Aerospace Structures,"Computers and Structures, v81, 2003, pp397-410.

[47] Papadrakakis, M. and Lagaros, N., "Reliability-based structural optimization using neutral networks and Monte Carlo simulation," Computer Methods in Applied Mechanics and Engineering, v191, 2002,pp3491-3507.

[48] Gasser,M. and Schueller ,G.I.,"Reliability-based optimization of structural systems," Mathematical Methods of Operations Research,v46,1997,pp287-307.

[49] Su, B., Rais-Rohani, M., and Singh, M.N., "Reliability-based optimization of anisotropic cylindrical shells with response surface approximations of buckling instability," in Proceedings of the 43'rd *AIAA/ASME/ASCE/AHS/ASC Structures,*

Structural Dynamics, and Material Conference, Denver, CO, April 22-25, Paper No.: AIAA-2002-1386, 2002.

[50] Nowak, A. S. and Collins, K. R., Reliability of Structures, McGraw Hill, Companies, Inc., Boston, 2000.

[51] Wu, Y.-T., "Computational methods for efficient structural reliability and reliability sensitivity analysis," *AIAA Journal*, Vol. 32, No. 8, August 1994, pp. 1717-1723.

[52] Vanderplaats ,G.N., "Numerical Optimization Techniques for Engineering Design", Third Edition.

[53] Madson, H. O., Krenk, S., and Lind, N. C., Methods of Structural Safety, Prentice-Hall, Inc., New Jersey, 1986, pp. 120-123.

[54] Liu,P.L, and Der Kiureghian, A., "Optimization algorithms for structural reliability," Structural Safety, v9,1991,pp161-177.

[55] Abdo,T. and Rackwitz,R , "A new beta point algorithm for large time-invariant and time variant reliability problems" ,Reliability and Optimization of Structural Systems'90:Proc.3rd WG 7.5 IFIP Working Conf., Berkeley ,1990,pp1-11.

[56] Noton, B.R., "ICAM: Manufacturing Cost/Design Guide," Final Report, Vol. I, II, and III, AFML-TR-76-227, Battelle's Columbus Laboratories, 1979.

[57] Noton, B.R., "ICAM Manufacturing Cost/Design Guide, Final Technical Report - Airframe User's Manual - Vol. I, II, and III," AFWAL-TR-83-4033, January 1983.

[58] Noton, B.R., "ICAM Manufacturing Cost/Design Guide, Vol. V - Machining," AFWAL-TR-83-4033, March 1985.

[59] Noton, B.R., "ICAM Manufacturing Cost / Design Guide, Volume I: Demonstration Sections," AFWAL-TR-80-4115, Sep. 1980.

[60] Frangopol, D., "Reliability-Based Optimum Structural Design," in Probabilistic Structural Mechanics Handbook, Theory and Industrial Applications, Edited by C. Sundararajan, Chapman & Hall Publishing Co., 1995.

[61] Haugen, E. B., Probabilistic Mechanical Design, John Wiley & Sons, 1980.

[62] Bralla, J. G., editor Design for Manufacturability Handbook, 2nd Edition, McGraw-Hill Publishing Co., 1998.

[63] Trucks, H. E., Designing for Economical Production, Society of Manufacturing Engineers, 2nd Edition, 1987.

[64] Dowling, N. E., Mechanical Behavior of Materials, 2nd Ed., Prentice Hall Publishers, 1998.

[65] Balasubramaniam, L., Producibility Analysis using Analytical and Empirical Process Models, PhD Dissertation, Department of Mechanical Engineering, MIT, 1993.

[66] Laue, K. and Stenger, H., Extrusion Processes, Machinery, Tooling, American Society for Metals, 1981.

[67] Niu, M. C. Y., Airframe Structural Design, Conmilit Press, LTD., 1988.

[68] Bruhn, Analysis and Design of Flight Vehicle Structures, S.R. Jacobs & Associates, 1972.

[69] Kuhn, P., Peterson, J. P., and Levin, L. R., "A Summary of Diagonal Tension: Part I - Methods of Analysis," NACA TN 2661, 1952.

[70] DOT, Design Optimization Tools, Version 5, Vanderplaats Research and Development, Colorado Springs, 2001.